universität wien

MASTERARBEIT / MASTER'S THESIS

Titel der Masterarbeit / Title of the Master's Thesis

"Pressure-induced polymorphism of anhydrous copper sulphate single crystals"

verfasst von / submitted by

Stefan Knesz, BSc

angestrebter akademischer Grad / in partial fulfilment of the requirements for the degree of

Master of Science (MSc)

Wien, 2021 / Vienna 2021

Studienkennzahl lt. Studienblatt / degree programme code as it appears on the student record sheet:	A 066 815
Studienrichtung lt. Studienblatt / degree programme as it appears on the student record sheet:	Erdwissenschaften
Betreut von / Supervisor:	Univ.-Prof. Dr. Ronald Miletich-Pawliczek

Abstract

Single crystals of anhydrous copper sulphate, $CuSO_4$, have been analysed by conducting high pressure experiments using a diamond anvil cell. Raman spectrometry and single crystal X-ray diffractometry have been performed at pressures up to approximately 8.5 GPa on isothermal compressions. While X-Ray diffraction was not able to distinctly confirm any phase transitions without doubt, Raman spectrometry suggests a phase transition around 1.5 GPa, most likely associated with a reduction in symmetry from Pnma to $P2_1/c$. In addition, a first order transition was found to occur between 7 and 8.5 GPa during compression and between 4.39 GPa and 1.98 GPa during decompression. It shows typical characteristics of a first order transition with a pronounced hysteresis and the critical transformation pressure P_c to occur within a range of P individually for each sample crystal. A coexistence of interspersed low and high-pressure domains similar to the occurrence of twin domains and polysynthetic twinning can be assumed. This second phase transition is accompanied by a reduction in symmetry from $P2_1/c$ to $P\bar{1}$.

Acknowledgement

I would first of all like to thank Prof. Ronald Miletich for the opportunity to work under his supervision on this difficult task and for the support to overcome numerous obstacles. Further I want to thank him for always providing me with productive input in many personal discussions and a comfortable working atmosphere.

My special thanks go to Dr. Martin Ende for introducing me to all of the laboratory devices and programs I needed and for the many hours he spent to figure out solutions for some of my technical problems.

I also want to thank Dr. Dominik Talla for providing me with more than enough sample crystals, which he always had an extra batch prepared in case of complications with my experiments.

I am grateful to Thomas Rosen, Wolfgang Prosche and Erich Polacek for providing liquid nitrogen when needed.

And finally, I especially want to thank my family for their support and patience during the last years.

Eidesstattliche Erklärung

Ich erkläre eidesstattlich, dass ich die vorliegende Arbeit selbständig und ohne unzulässige Hilfsmittel angefertigt habe. Die verwendeten Quellen sind vollständig zitiert.

Statement under Oath

I declare on oath that I have authored this thesis independently and without undue help of any kind. All sources are fully cited.

Table of Content

1. Introduction

The increasing demand of electricity in the world and the growing awareness concerning environmental and climate change leads to a major change in mind. Instead of building new powerplants, people now search for innovative routes to improve the efficiency of already existing facilities and reduce unnecessary energy losses, and harvest energy from various sources. In this context Müller et al. (2020) investigated the capability of different substances of storing heat energy by using the concept of thermo chemical energy storage (Cot-Gores et al., 2012; Lele 2016; Prieto 2016). Here, thermal energy is stored either through chemical sorption processes or a reversible chemical reaction. Aim of current research initiatives is to find novel storage materials, which can store the energy released during these chemical reactions while maintaining a stable state in a more efficient way together with providing high energy densities and the capability for cycling the process.

Numerous current studies already investigated the physical and chemical properties of different sulphates, especially in the field of planetary mineralogy (e.g.: Comodi et al., 2021; Vaniman et al., 2004). For this study sulphates have shown to be suitable candidates as their properties allow the storage of reaction energy without becoming unstable. Moreover, anhydrous copper sulphate poses a specifically promising material (Müller et al. 2021) considering the energy density released in the context of ammonization reactions. When combined with ammonia, anhydrous copper sulphate forms a tetraamine complex, a structure where four NH_3 molecules are integrated into the crystal structure. This chemical reaction is fully reversible, meaning it can be reversed with little energy loss and release the energy which was stored beforehand due to the formation of the tetraamine complex very fast, making it an applicable material for this study. Information about the behaviour of anhydrous copper sulphate ($CuSO_4$) as well as anhydrous copper tetraamine sulphate ($Cu(NH_3)_4SO_4$) is crucial for further applications under high-temperature and high-pressure conditions.

Copper sulphate, especially in its hydrous form of copper sulphate pentahydrate ($CuSO_4{\cdot}5H_2O$), has many different applications in a broad spectrum of fields. It is used as a crop protection agent as it has fungicidal properties (Johnson 1935), as an important chemical reactant (Benedict 1909), as an inhibitor of algae growth in swimming pool water additives (Gibson 1972) and is also used in the medical field.

Furthermore, anhydrous copper sulphate can be used as a drying agent (Sushanthi et al., 2020; Hoffman et al., 1980). Despite its many applications and widespread use, many physical properties and crystal-structural behaviour of copper sulphate remain unknown or poorly understood. Especially many detail properties are still undiscovered about anhydrous copper sulphate leaving room for future. There are several studies concerning polymorphism of the members of this isomorphous sulphate series, which often talk about three phases in dependence of pressure and temperature (Pistorius, 1961; Dunitz and Pauling, 1965; Wehner, 1976). Most of these studies are solely based on powder X-ray diffraction and are therefore of limited use. The lack of research regarding $CuSO_4$ can be explained by its difficult and unstable nature in combination with water, as even with the slightest contamination with water the anhydrous copper sulphate forms copper sulphate pentahydrate, thus making experimentation with the substance a complex process.

This study specifically examines the properties of anhydrous $CuSO_4$ under water-free high-pressure conditions. Anhydrous copper sulphate was first described by Scacchi (1873) on a natural specimen from Mount Vesuvius, which he named hydrocyanite. Later it was renamed to chalcocyanite, due to the inappropriateness of the term “hydro” in combination with an anhydrous substance. Kokkoros and Rentzeperis (1958) defined a unit cell and space group for the first time and determined the crystal structure, which were later refined by Wildner and Giester (1988) to:

a = 8.409 Å, b = 6.709 Å, c = 4.833 Å and Z = 4.

2. Methodology

2.1. Synthesis

The sample crystals were synthesized by Dr. Dominik Talla the same way, they were for an earlier study of anhydrous copper sulphate by Wildner and Giester (1988). $CuSO_4 \cdot H_2O$ was mixed with H_2SO_4 in Teflon lined steel vessels and heated to 500K for one week. After cooling colourless $CuSO_4$ crystals had formed.

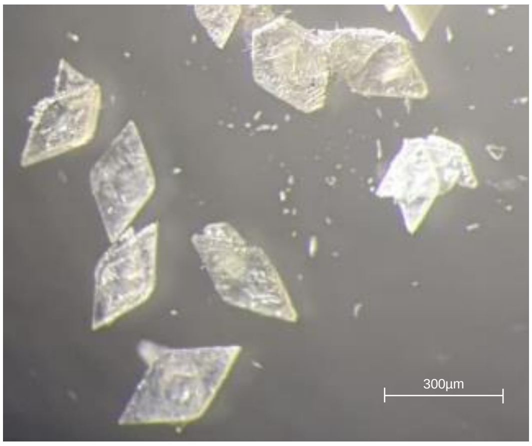

Figure 1: synthetic anhydrous CuSo4 single crystals

2.2. High-Pressure Diamond Anvil Cell

Diamond anvil cells (DAC) are the easiest and most practical way to apply very high hydrostatic pressures on samples. It is possible to apply this technique in the Mbar region of pressure and therefore easy to simulate conditions in the interior of the Earth. One of the biggest advantages is, that the sample is still visible even under pressure through a hole in the cell in which the diamonds themselves act like windows.

For this thesis DACs of the type ETH (Allan et al., 1996, Miletich et al., 2000) with Böhler-Almax cut diamond anvils were used. In this case the diamonds are mounted directly on tungsten carbide and held in place with glue. A 250 µm thick pre-cut steel square served as gasket. By applying pressure with the DAC, a 100 µm thick area has been pre-imprinted, before a hole with 250 µm in diameter was drilled in the centre of the indent using a spark eroder of the type BETSA-MH20M.

2.3. Sample preparation under inert-gas atmosphere

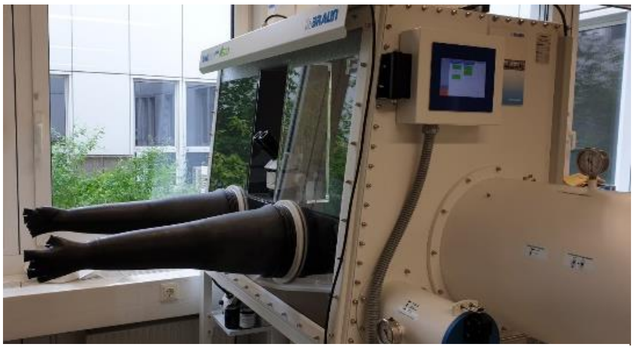

Figure 2: MBRAUN UNIlab Plus glovebox

Being highly hygroscopic, the crystalline substance had to be mounted under inert gas conditions in a glovebox type MBRAUN UNIlab Plus was necessary. Within the pure argon atmosphere (with less than 0.5 ppm H_2O and O_2) the sample was stable and safe to handle. A single crystal fragment of anhydrous $CuSO_4$ and one fragment of a synthetic quartz standard and three ruby spheres were mounted on one of the diamond anvils. Then the DAC was closed, before taking it out of the glovebox, in order to isolate the sample from air humidity.

2.4. Cryoloading

Figure 3: Flooding of the DAC with liquid argon

Because of the hygroscopic nature of the sample, it was not possible to use ethanol-methanol as pressure transmitting medium (Klotz et al., 2009). Cryoloading with liquid argon (Mao and Bell 1980) had been chosen as an alternative. For this process a steel cylinder was placed in a polystyrene container filled with liquid nitrogen. The closed DAC as transferred from the glovebox was placed inside the cylinder. The liquified nitrogen was used to cool down the steel vessel. Then the cylinder was flooded with argon gas and the screws were loosened a bit (half a rotation). After five to ten minutes enough argon has condensated and the level of liquified Ar was that high to fully submerge the sample chamber. Now the anvils could be pulled apart in order to fill the pressure chamber with fluid pressure medium. Finally, the DAC was deliberately closed by overturning the screws for approximately a quarter rotation.

2.5. X-Ray Diffractometry

A DAC was prepared with a $CuSO_4$ crystal fragment together with a quartz crystal serving as pressure standard. Additionally, three ruby spheres were put inside the chamber to be able to adjust the pressure by checking on the Raman spectrometer. Later the pressure was precisely determined by using the volume of the quartz unit cell with the EoSFit7 PV/PVT Calculator, setting up a third order Birch-Murnaghan-Equation of state (BM-EOS) (Angel et al., 1997; Scheidl et al, 2016).

Before starting the actual series of measurements, the orientation matrices of both crystals had to be determined. Therefore, the DAC was mounted on a STOE StadiVari X-ray Diffractometer with an open Eulerian Cradle, a Dectris Pilatus 300k detector and a MoKα microfocus X-ray tube as source. The device was operated by using the X-Area 1.7.2 software (Stoe & Cie GmbH).

A second diffractometer of the type Stoe AED 2 was used to determine the precise lattice parameters through high-resolution profiles. This diffractometer is equipped with a closed Eularian Cradle and equipped with a point detector and has a MoKα X-ray tube as source installed. The STOE AED 2 was controlled via the Single 2012 software (Angel & Finger, 2011). To enhance the quality of the data as much as possible, the orientation matrix was re-determined performing 8-position-centering (King and Finger, 1979) in order to determine the setting angles of maximum 21 reflection before each new pressure step.

The acquired data of the diffractometer was then further processed by conducting unconstrained and constrained least squares refinements as well as fitting an Equation of State (EOS) to the unit cell parameter. A third order Birch-Murnaghan-EOS (BM3-EOS) has been determined by using EoSFIT7-GUI (Gonzales-Platas, 2016)

Birch (1947) extended the Murnaghan-Equation of state by adding the finite Eulerian strain.

$$P = \frac{3}{2}K_{T0}\left[\left(\frac{V_0}{V}\right)^{\frac{7}{3}} - \left(\frac{V_0}{V}\right)^{\frac{5}{3}}\right] \times \left\{1 + \frac{3}{4}(K'_{T0} - 4)\left[\left(\frac{V_0}{V}\right)^{\frac{2}{3}} - 1\right]\right\} \quad \text{(Equation 2)}$$

The third order BM-EOS can only be reduced to second order, if the value of the first derivate of the isothermal bulk modulus K' is fixed to 4 (Angel et al., 2000).

$$P = \frac{3}{2}K_{T0}\left[\left(\frac{V_0}{V}\right)^{\frac{7}{3}} - \left(\frac{V_0}{V}\right)^{\frac{5}{3}}\right] \quad \text{(Equation 2)}$$

For more information about the derivation of BM-EOS see Katsura and Tange (2019)

2.6. Raman Spectroscopy

For the Raman spectroscopy a DAC was loaded with three different $CuSO_4$ crystal fragments of unspecific orientation and again three ruby spheres for pressure determination. The spectra were acquired from a Horiba Jobin Yvon LabRAM-HR 800 Raman spectrometer. To be able to focus the beam into the pressure chamber of the DAC, a long-distance objective from type Olympus LMPlanFL N 50x mounted on an Olympus BX41 microscope, which itself is attached to the spectrometer, was used.

The devices were operated by the LabSpec 6 Software (Horiba Scientific). A He-Nd laser with 632nm wavelength was chosen as excitation laser source. To improve the quality of the spectra an acquisition time of 40 seconds with an 1800 lines per mm grating was used. To further refine and fit the spectra the PeakFit v4.12 Software (Systat Software, Inc) was used with the Gauss-Lorentz-Area Method.

For the pressure calculation the rubies were measured at room pressure and the Raman shift of the R_1 luminescence lines were taken as calculation basis. After each increase or decrease of pressure, a ruby spectrum was measured and fitted. The wavenumber of the R_1 line then can be used to determine the pressure by inserting in the empirical formula by Mao et. al. (1986).

$$P = \frac{A}{B}\left\{\left[1 + \left(\frac{\Delta\lambda}{\lambda_0}\right)\right]^8 - 1\right\} \quad \text{(Equation 3)}$$

A…19.04Mbar
B…7.665Mbar
λ…wavelength of

3. Results and Discussion

3.1. X-ray Diffraction and lattice parameters

The pressure was first reduced to 1.41 GPa before increasing it to 8.55 GPa. An additional data point measured at ambient pressure (personal communication Ende) has been added into all of the following diagrams (Figures 4 – 7, 8 and 9).

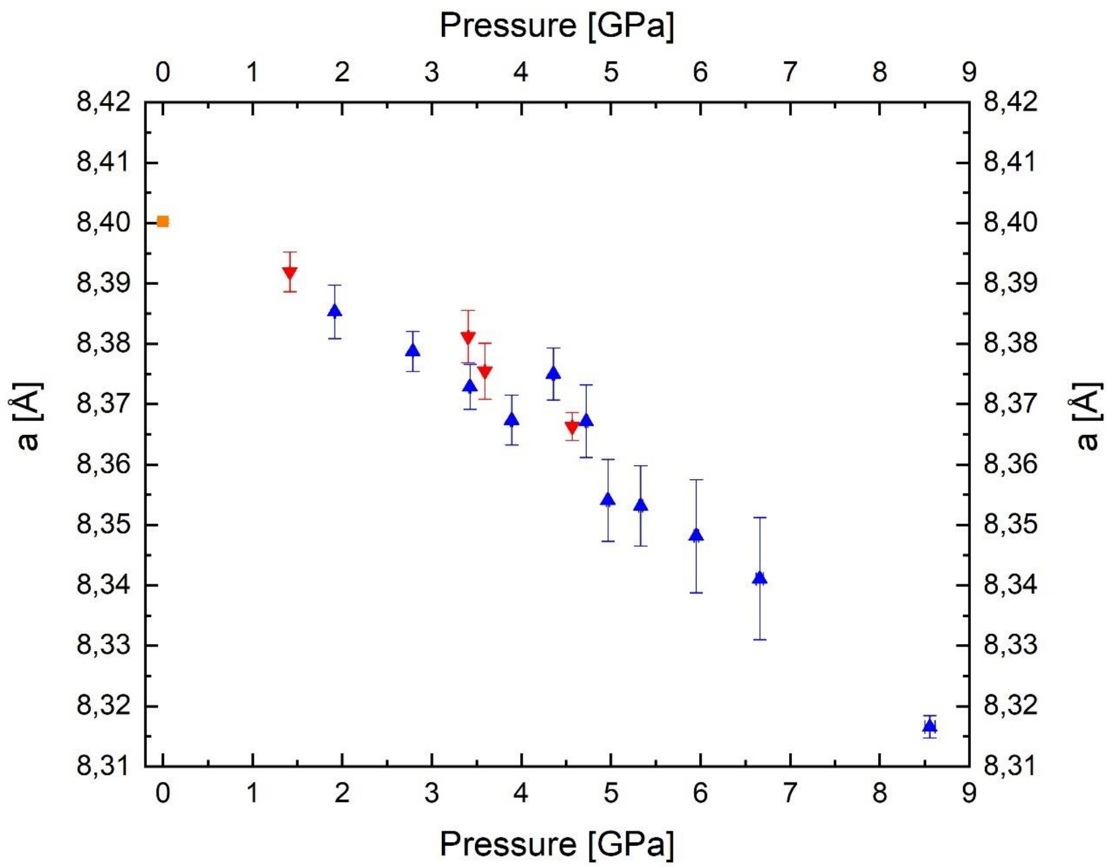

Figure 4: lattice parameter a. The red triangles indicate the decompression steps from 4.56 GPa to 1.41 GPA, while the blue triangles show the subsequent compression to 8.55 GPa. The orange square represents the additional datapoint at ambient pressure.

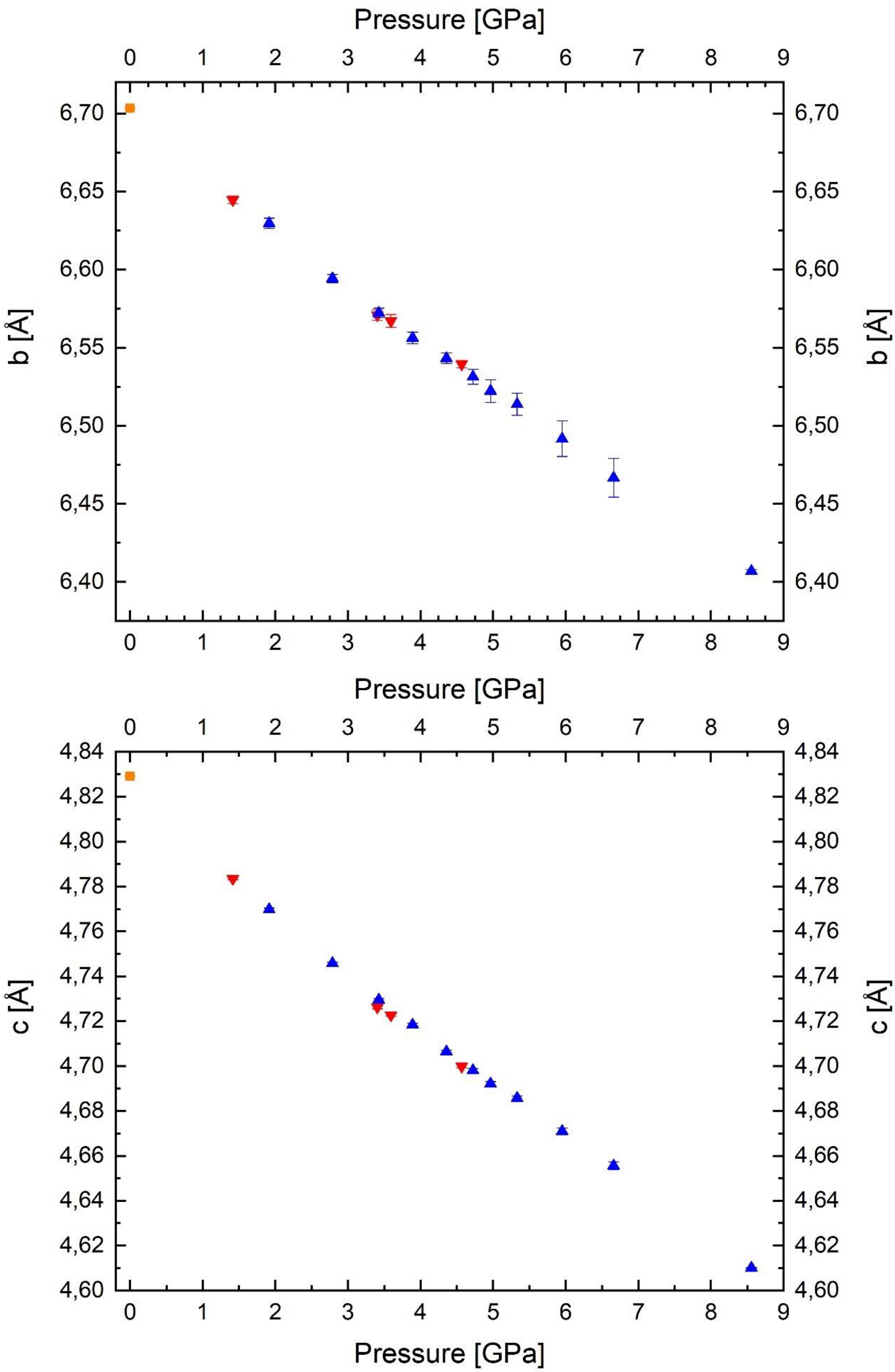

Figure 5: lattice parameters b (top) and c (bottom). The red triangles indicate the decompression steps from 4.56 GPa to 1.41 GPA, while the blue triangles show the subsequent compression to 8.55 GPa. The orange square represents the additional datapoint at ambient pressure.

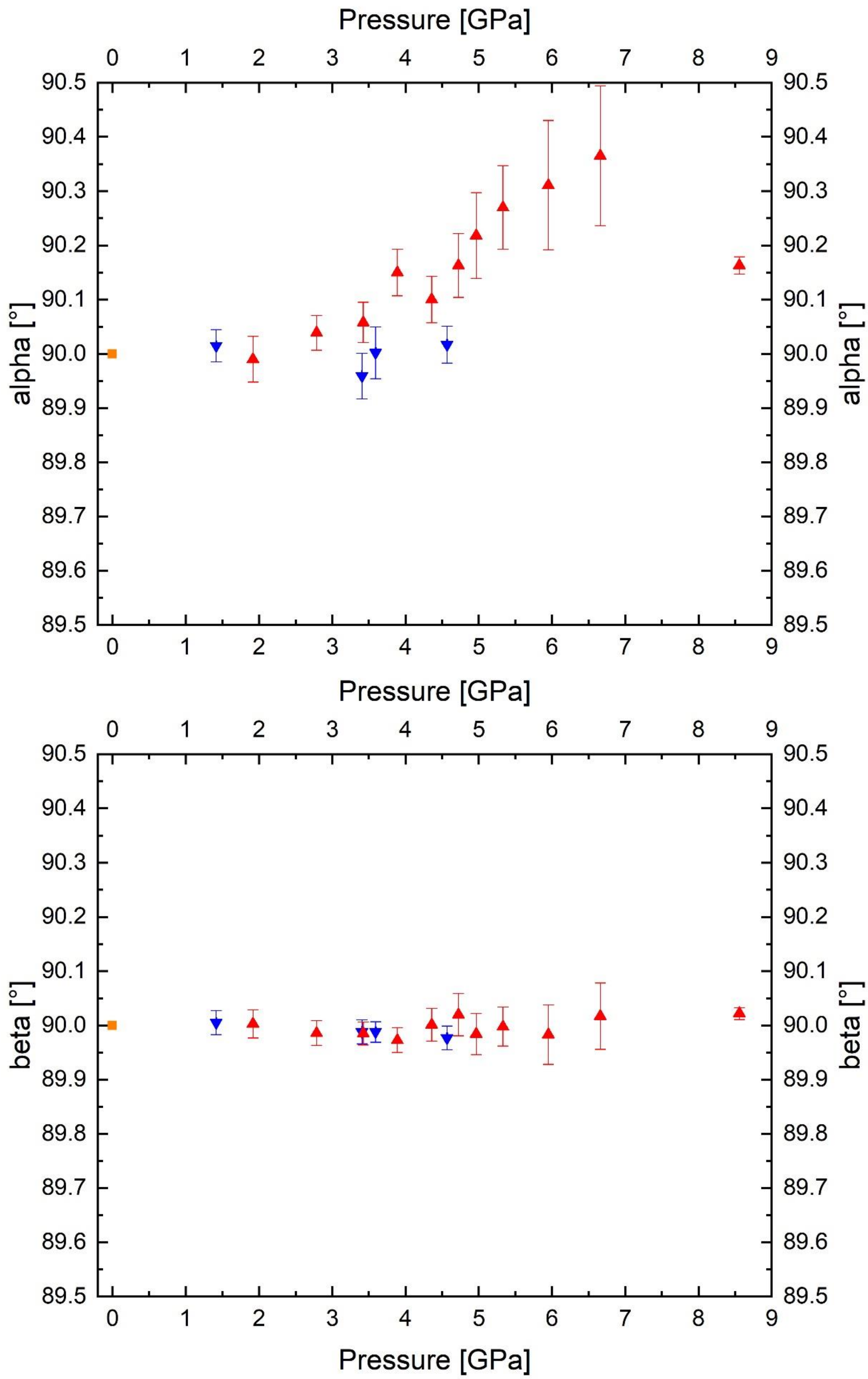

Figure 6: lattice parameter alpha (top) and beta (bottom). The red triangles indicate the decompression steps from 4.56 GPa to 1.41 GPA, while the blue triangles show the subsequent compression to 8.55 GPa. The orange square represents the additional datapoint at ambient pressure.

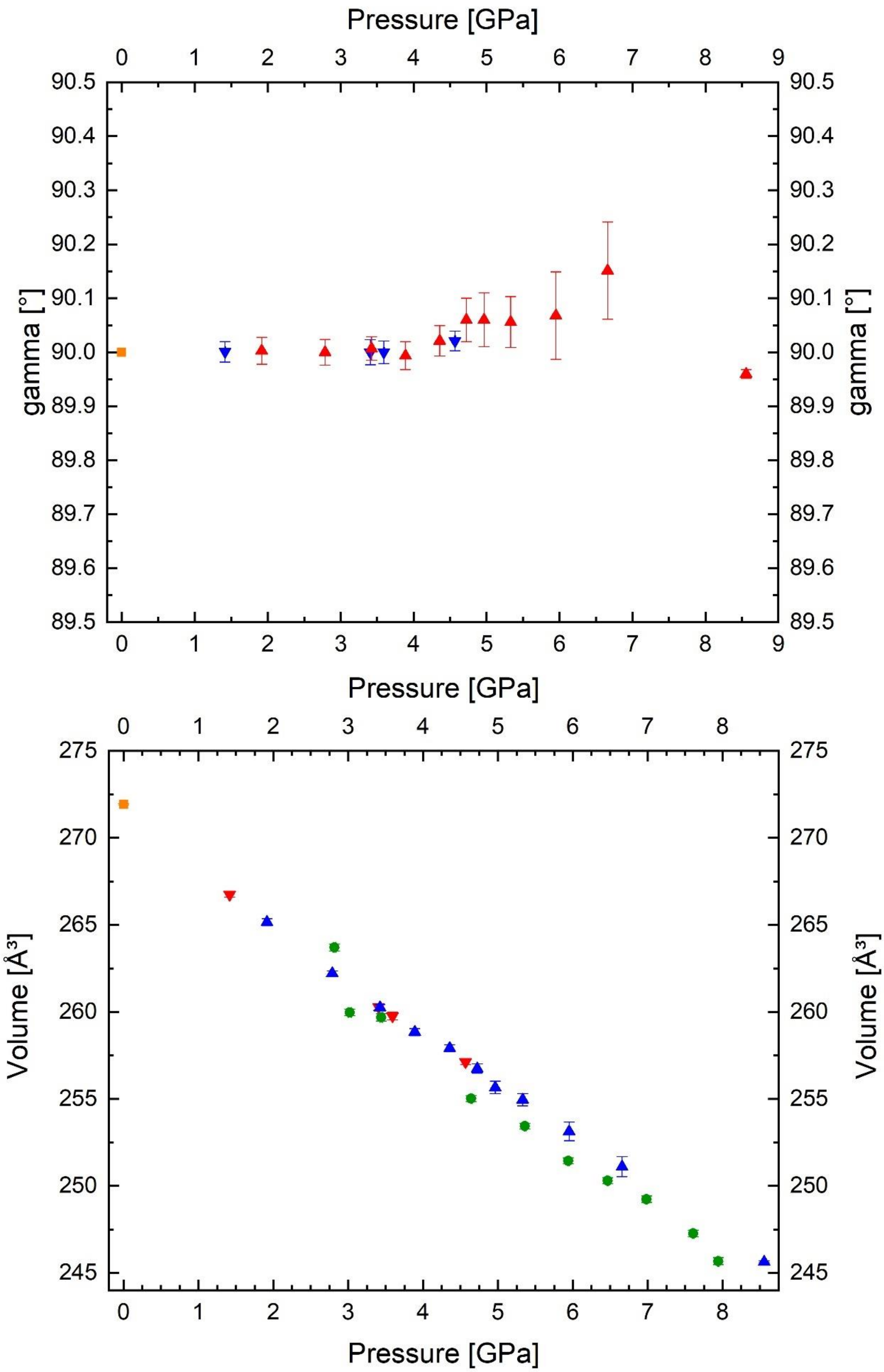

Figure 7: lattice parameter gamma (top) and the volume (bottom). The red triangles indicate the decompression steps from 4.56 GPa to 1.41 GPA, while the blue triangles show the subsequent compression to 8.55 GPa. The orange square represents the additional datapoint at ambient pressure and the green circles represent an additional data set, measured during decompression (personal communication Ende)

V_{Quartz} [Å^3]	Druck [GPa]	a [Å]	b [Å]	c [Å]	alpha [°]	beta [°]	gamma [°]	V [Å^3]
102.973(11)	4.567(7)	8.3663(23)	6.5392(23)	4.6998(6)	90.021(18)	89.977(22)	90.017(18)	257.13(16)
104.661(11)	3.592(6)	8.3754(46)	6.5672(41)	4.7227(4)	90.000(21)	89.988(19)	90.002(21)	259.76(22)
105.002(11)	3.406(6)	8.3812(43)	6.5709(34)	4.7262(6)	90.000(23)	89.988(22)	89.959(23)	260.28(19)
109.166(12)	1.416(5)	8.3919(33)	6.6446(23)	4.7835(5)	90.001(19)	90.005(22)	90.015(19)	266.74(14)
108.015(25)	1.917(12)	8.3853(44)	6.6296(33)	4.7697(6)	90.003(25)	90.003(26)	89.990(25)	265.15(20)
106.187(12)	2.788(6)	8.3787(32)	6.5942(26)	4.7457(6)	90.000(24)	89.986(23)	90.039(24)	262.20(15)
104.967(25)	3.425(14)	8.3728(37)	6.5723(30)	4.7294(5)	90.007(22)	89.985(21)	90.058(22)	260.25(17)
104.128(21)	3.890(12)	8.3673(41)	6.5562(37)	4.7183(5)	89.994(26)	89.973(23)	90.150(26)	258.84(20)
103.325(24)	4.356(14)	8.3750(43)	6.5432(33)	4.7064(6)	90.021(28)	90.001(30)	90.100(28)	257.90(20)
102.716(21)	4.724(13)	8.3671(60)	6.5314(48)	4.6981(8)	90.060(40)	90.020(39)	90.163(40)	256.74(27)
102.330(27)	4.964(17)	8.3541(68)	6.5221(73)	4.6921(9)	90.060(50)	89.984(38)	90.218(50)	255.65(36)
101.755(35)	5.331(22)	8.3531(66)	6.5138(71)	4.6857(9)	90.056(47)	89.998(36)	90.270(47)	254.95(35)
100.824(40)	5.951(27)	8.3481(93)	6.4916(114)	4.6709(15)	90.068(81)	89.983(55)	90.311(81)	253.13(54)
99.815(55)	6.659(40)	8.3410(101)	6.4666(123)	4.6556(16)	90.151(90)	90.017(61)	90.365(90)	251.11(58)
97.348(70)	8.557(57)	8.3165(18)	6.4068(10)	4.6100(1)	89.960(8)	90.022(11)	90.163(8)	245.63(7)

Table 1: unit cell parameters of $CuSO_4$ plotted in figure 22 and 23. The pressure was calculated from the measured unit cell volume of the quartz crystal.

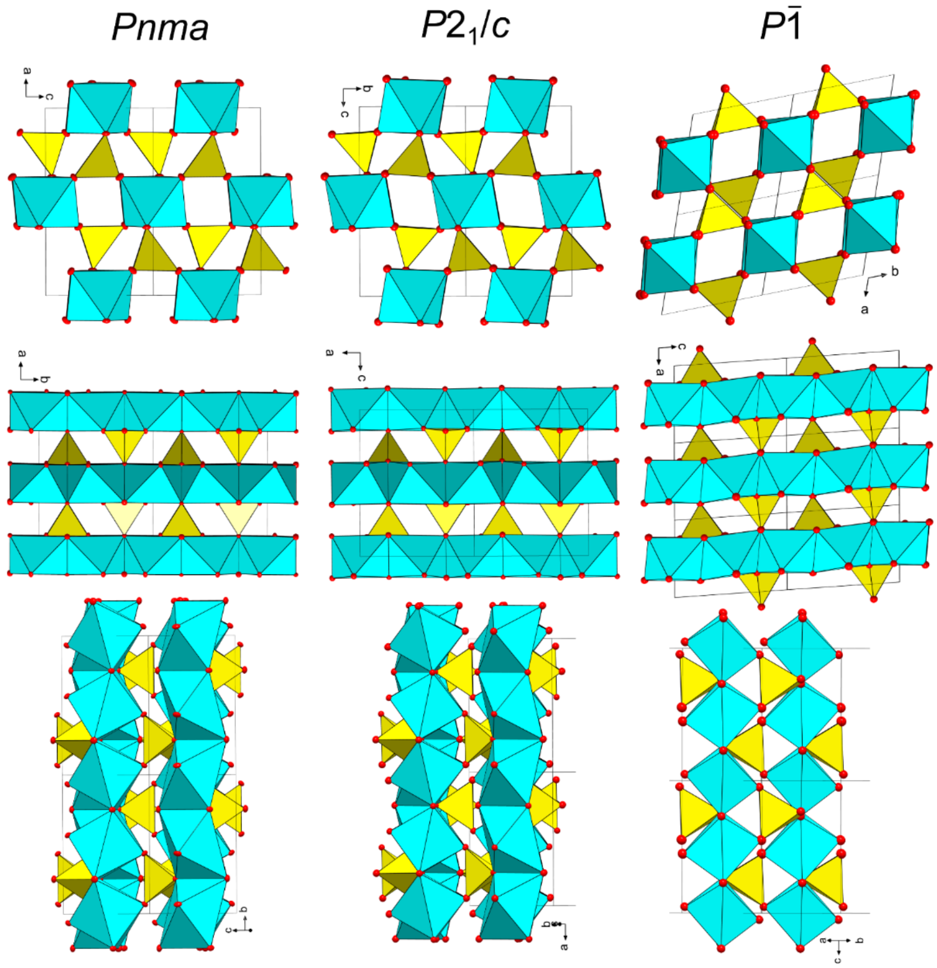

Figure 8: graphical demonstration of the three phases of anhydrous $CuSO_4$ (personal communication Ende, 2020)

Figure 8 shows the comparison of the three phases of $CuSO_4$ involved, with a first phase transition from orthorhombic Pnma to monoclinic $P2_1/c$ and a second phase transition from monoclinic $P2_1/c$ to triclinic $P\bar{1}$. As the figure shows, no change of coordination and no significant variation of the stereochemistry. Only the bonding angles and thus the volume change, however if plotted, the lattice parameters show now explicit irregularities (figures 4-7). In the following section equations of state have been fitted to enhance the significance even more.

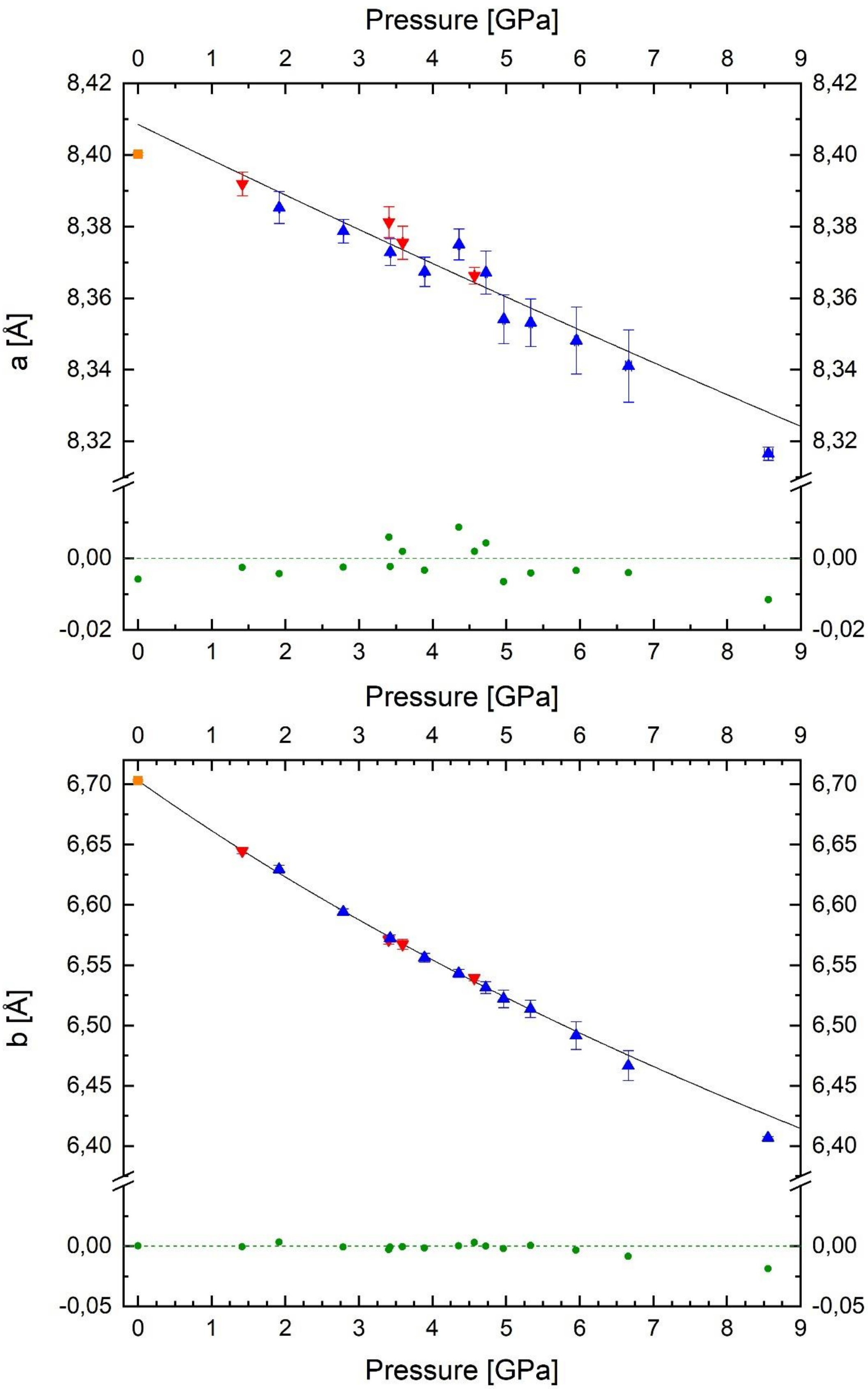

Figure 9: a BM2-EOS of state has been fitted for the lattice parameter a (top) and a BM3-EOS has been fitted for the lattice parameter b (bottom). A difference curve has been added in green to visualise the deviation of the measured data from the fitted EOS.

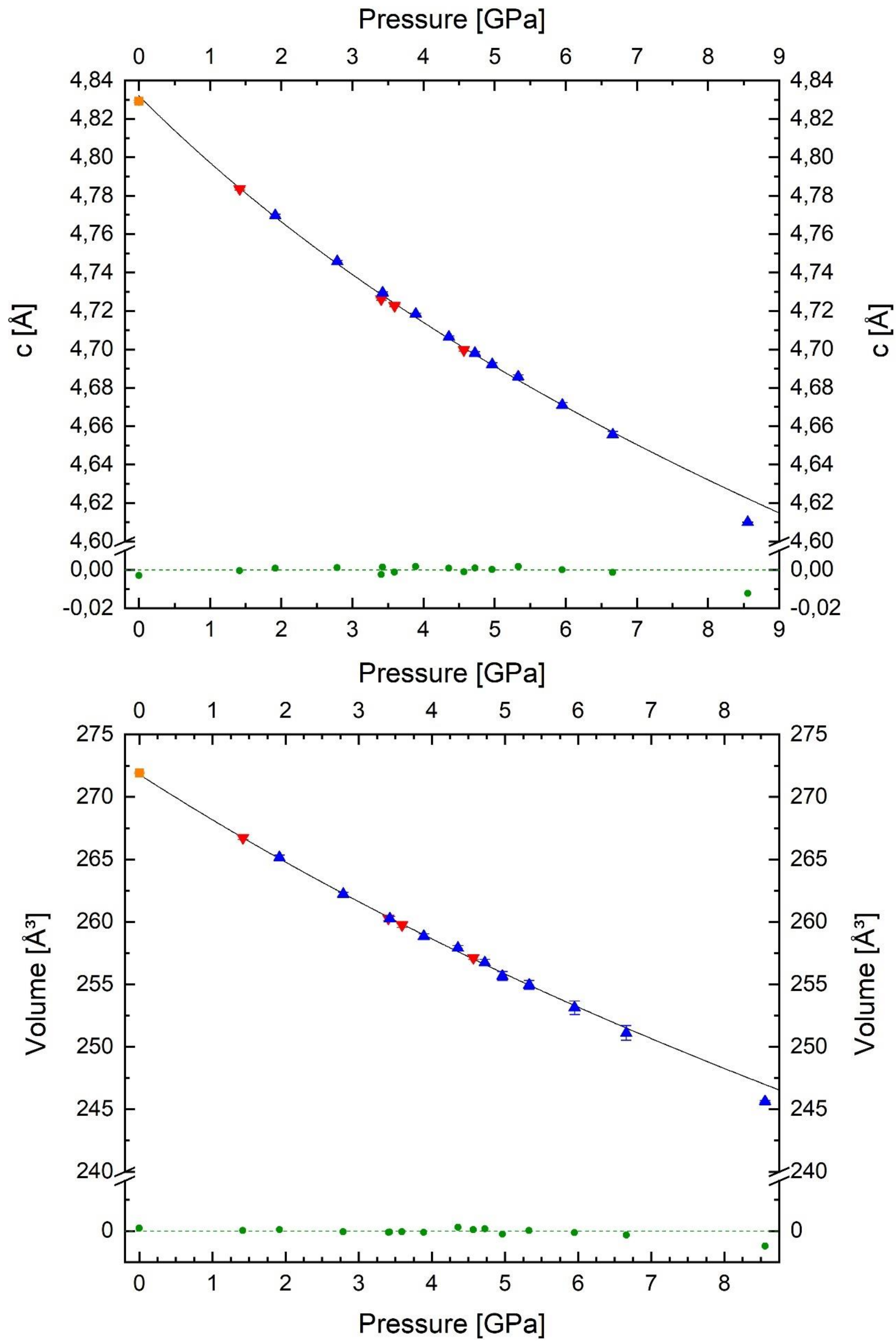

Figure 10: a BM3-EOS has been fitted for the lattice parameter c (top) and a BM2-EOS has been fitted for the unit cell volume (bottom). A difference curve has been added in green to visualise the deviation of the measured data from the fitted EOS.

Lattice Parameter	EOS	L_0 [Å]	M_0 [GPa]	M’	W-χ^2
a	BM2	8.408(3)	840.1(92.9)	12 (fixed)	1.02
b	BM3	6.703(8)	154.3(23.3)	12.7(7.9)	0.4
b	BM2	6.702(3)	156.5(4.3)	12 (fixed)	0.38
c	BM3	4.832(4)	129.4(12.8)	18.0(4.7)	4
c	BM2	4.827(1)	146.7(2.5)	12 (fixed)	4.56
Lattice Parameter	**EOS**	**V_0 [Å^3]**	**K_0 [GPa]**	**K’**	**W- χ^2**
volume	BM2	271.71(19)	73.5(1.3)	4 (fixed)	0.45
volume	BM3	271.8(4)	72.1(6.4)	4.4(2.1)	0.47

Table 2: Equation of state results for the lattice parameters a, b, c and the volume. L_0 and V_0 correspond to the initial values at P=0. M_0 and K_0 are the axial moduli and the bulk modulus, M’ and K’ correspond to their pressure derivatives. W-χ^2 = weighted chi squared value of the fit

With the acquired data from the Raman spectrometry as well as the structural data, measured and processed by Ende (personal communications) (figure 8), it can be assumed that all X-ray diffraction data points, except the ones at 8,55 GPa and ambient pressure, resemble the medium pressure phase with a monoclinic symmetry. By using the EoSFIT7-GUI (Gonzales-Platas, 2016), equations of state were fitted to the lattice parameter a, b and c and the unit cell volume. A 2nd order Birch-Murnaghan equation of state had to be fitted for parameter a to provide a meaningful result. For b and c third order Birch-Murnaghan equation of states were fitted respectively. To the volume a 3rd order Birch-Murnaghan equation of states had been fitted first, but as this results in K’=4.4 with an estimated standard deviation of 2.1, a 2nd order equation of state was fitted with a fixed value of 4 for K’ instead. Additionally, difference curves were implemented into the EOS diagrams (figures 9 and 10) to visualise the deviation of the measured data points from the fitted equations of state. The data also show, that in the direction of lattice parameter a, which is the direction of the octahedral chains, the compressibility is five times lower than for b and c, while it is approximately equal between b and c considering the errors (see table 2).

All lattice parameters show that the 8.55 GPa measurement lies beneath the fitted trendline of the equations of state. This monoclinic-triclinic phase transformation can also be confirmed by the Raman spectrometry data and would be expected to take place somewhere between 7 and 8.5 GPa.

Although the orthorhombic-monoclinic phase transition is known from the structural measurements (see figure 8) and the Raman spectroscopy data (see section 3.2.), no evidence has been found in the lower pressure region of the X-ray diffraction data.

3.2. Raman Spectra

Compression series starting at 0.47 GPa and going up to 8.49 GPa with the associated decompression series back to 1.15 GPa have been recorded on each of the three sample crystals mounted in the DAC. Additional reference measurements at room pressure were conducted in an argon atmosphere before starting to compress the sample.

After the first decompression step releasing from 8.49 GPa to 8.06 GPa the DAC was held at this state for nine days in total before continuing decompressing. To show the time dependence of the phase transition a spectrum was recorded on the same day, after one day, after five days and after nine days, resulting in a time-depending transformation towards the triclinic high-pressure phase. The compression as well as the decompression were each recorded in a continuous series without interruption to eliminate offset errors between spectra. To be able to allocate possible phase transitions precisely, the pressure steps were relatively small. For exact comparison the Raman spectra have been put together in three different stack plots, showing the compression series, the decompression series and the pause between the two series, ranging from 7.05 GPa (compression) to 7.05 GPa (decompression), respectively.

Additionally, the fitted peak positions have been plotted in three diagrams ranging from 100 cm^{-1} to 1250 cm^{-1}. The individual Raman bands have been labelled according to their starting Raman shift position of their respective series in [cm^{-1}]. A " * " symbol at the end of the Raman band label indicates peak position data originating from the decompression series.

The following Raman spectra have been compared with Fu et al. (2012) to distinguish which Raman bands can be attributed to the SO_4-modes. Bands around 450 to 500 cm^{-1} = v_2 of SO_4, around 600 cm^{-1} = v_4, around 930 cm^{-1} = v_1 and bands around 1150 to 1250 cm^{-1} = v_3. Raman bands below 400 cm^{-1} can be most likely correlated with various copper vibrations.

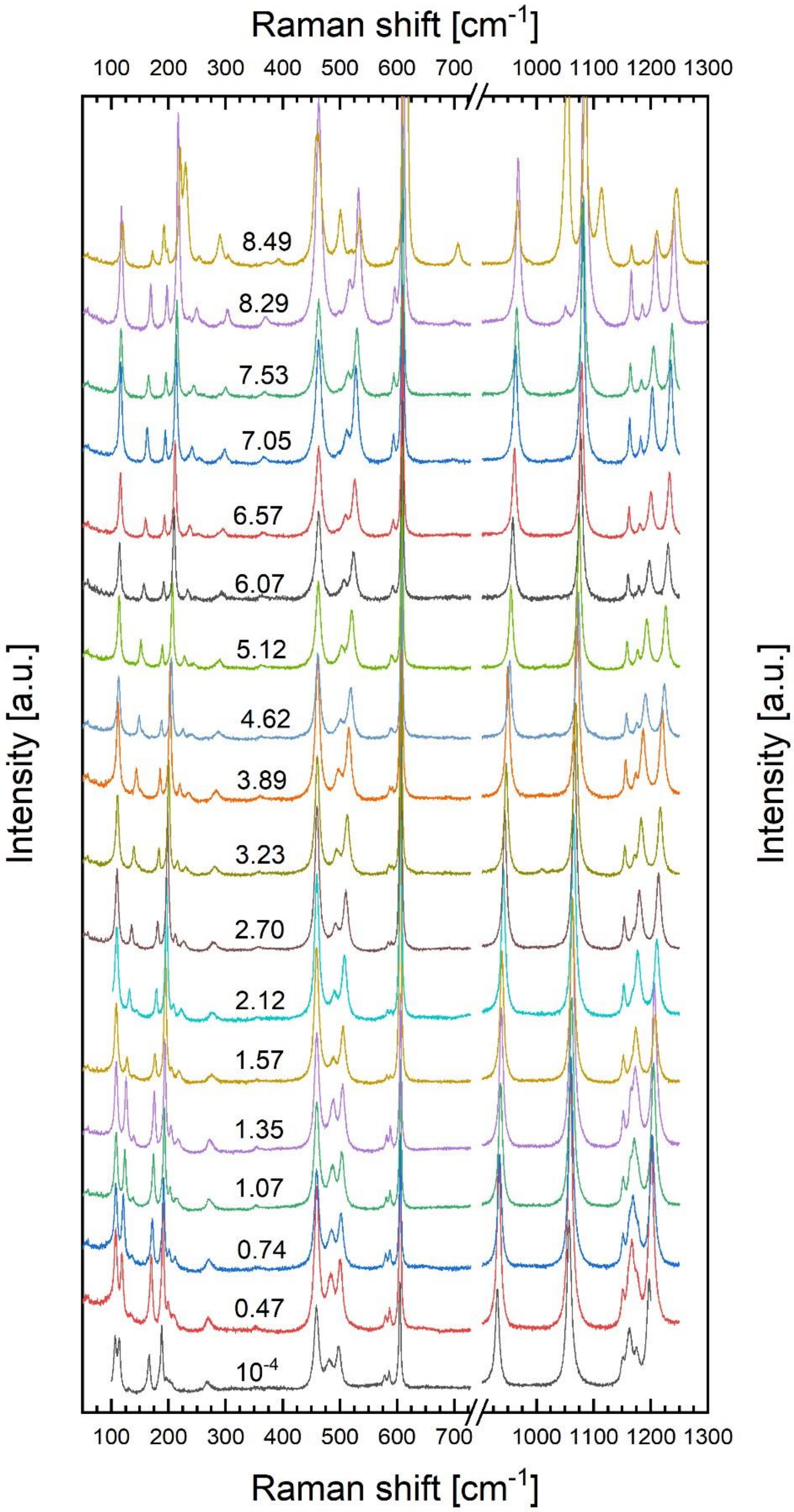

Figure 11: Stacked plot of the Raman spectra of $CuSO_4$ crystal 1, obtained during the compression series, showing changes of Raman bands under increasing hydrostatic pressure. Each spectrum is labelled with the respective pressure in GPa.

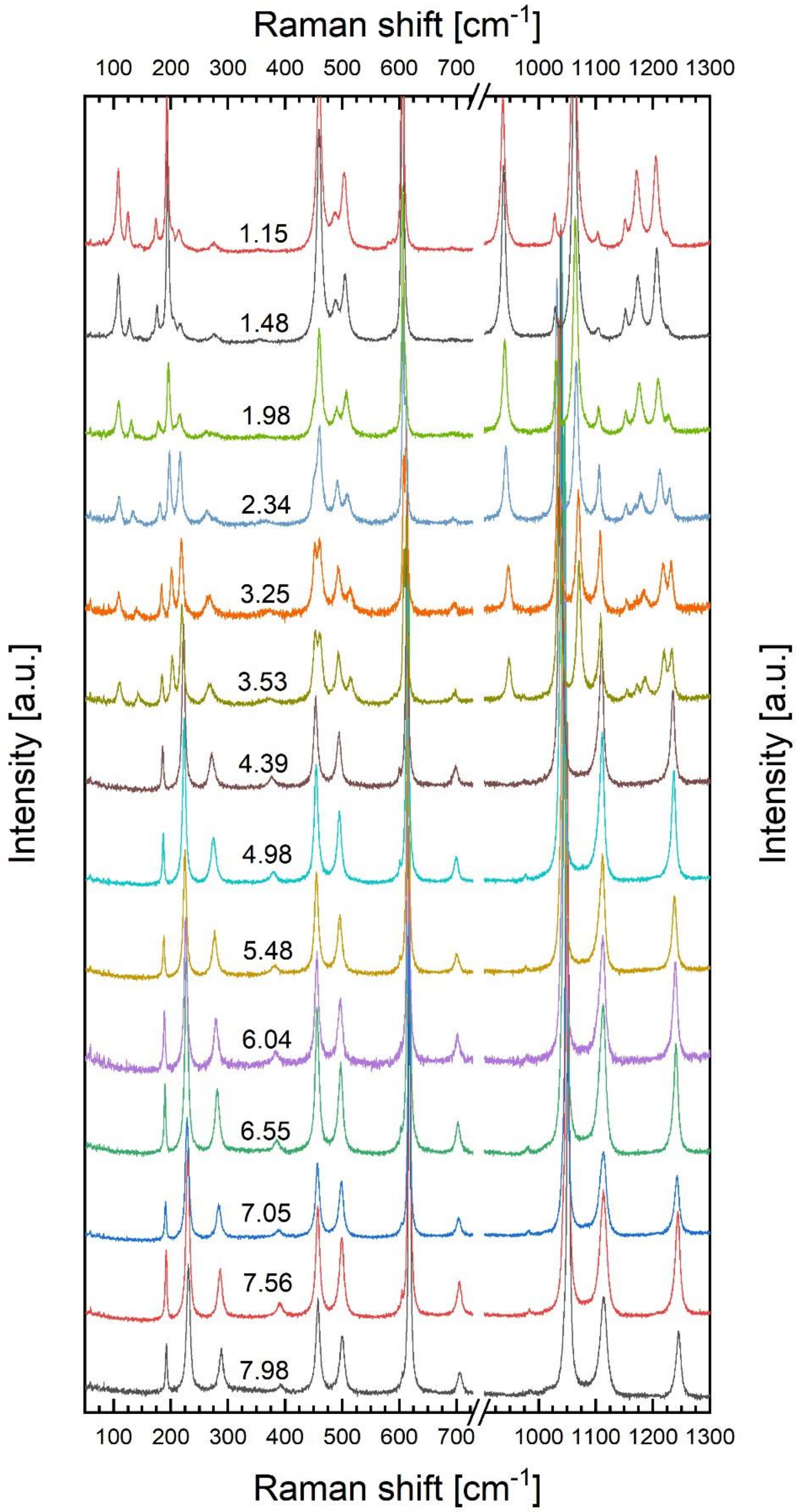

Figure 12: Stacked plot of the Raman spectra of $CuSO_4$ crystal 1, obtained during the decompression series, showing changes of Raman bands under decreasing hydrostatic pressure. Each spectrum is labelled with the respective pressure in GPa.

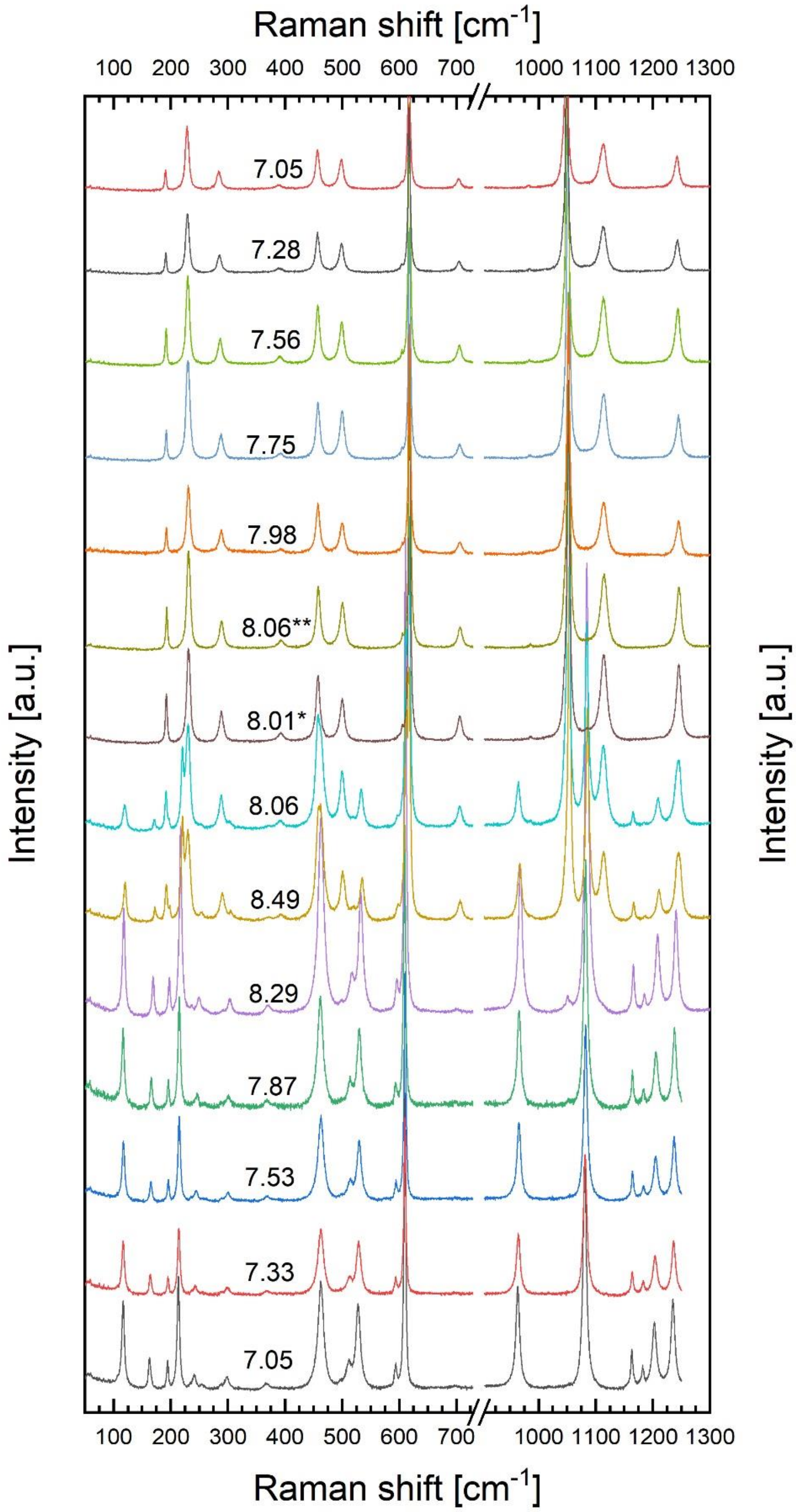

Figure 13: Stacked plot of the Raman spectra of $CuSO_4$ crystal 1, showing changes of Raman bands between the end of the compression and the start of the decompression series. Each spectrum is labelled with the respective pressure in GPa.

*: measured after 1 day; **: measured after 5 days

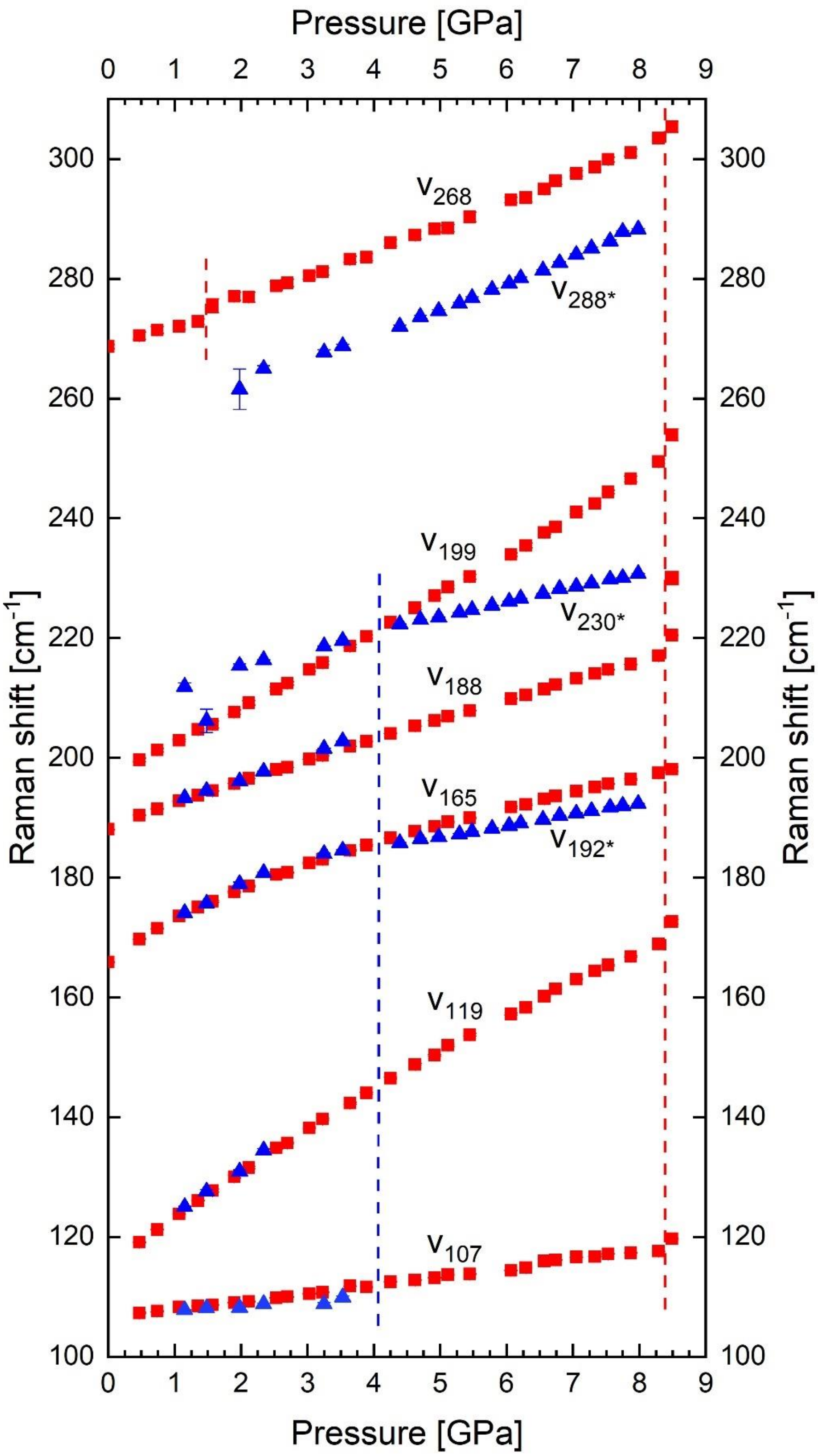

Figure 14: The evolution of the peak positions as a function of P during the compression series (red squares) and decompression series (blue triangles) of crystal 1. Vertical error bars represent the standard deviation of the exact peak position, while horizontal error bars represent the standard deviation of pressure. The red dotted line represents the P_c for a phase transition during the compression series, the blue dotted line represents the P_c during the decompression series.

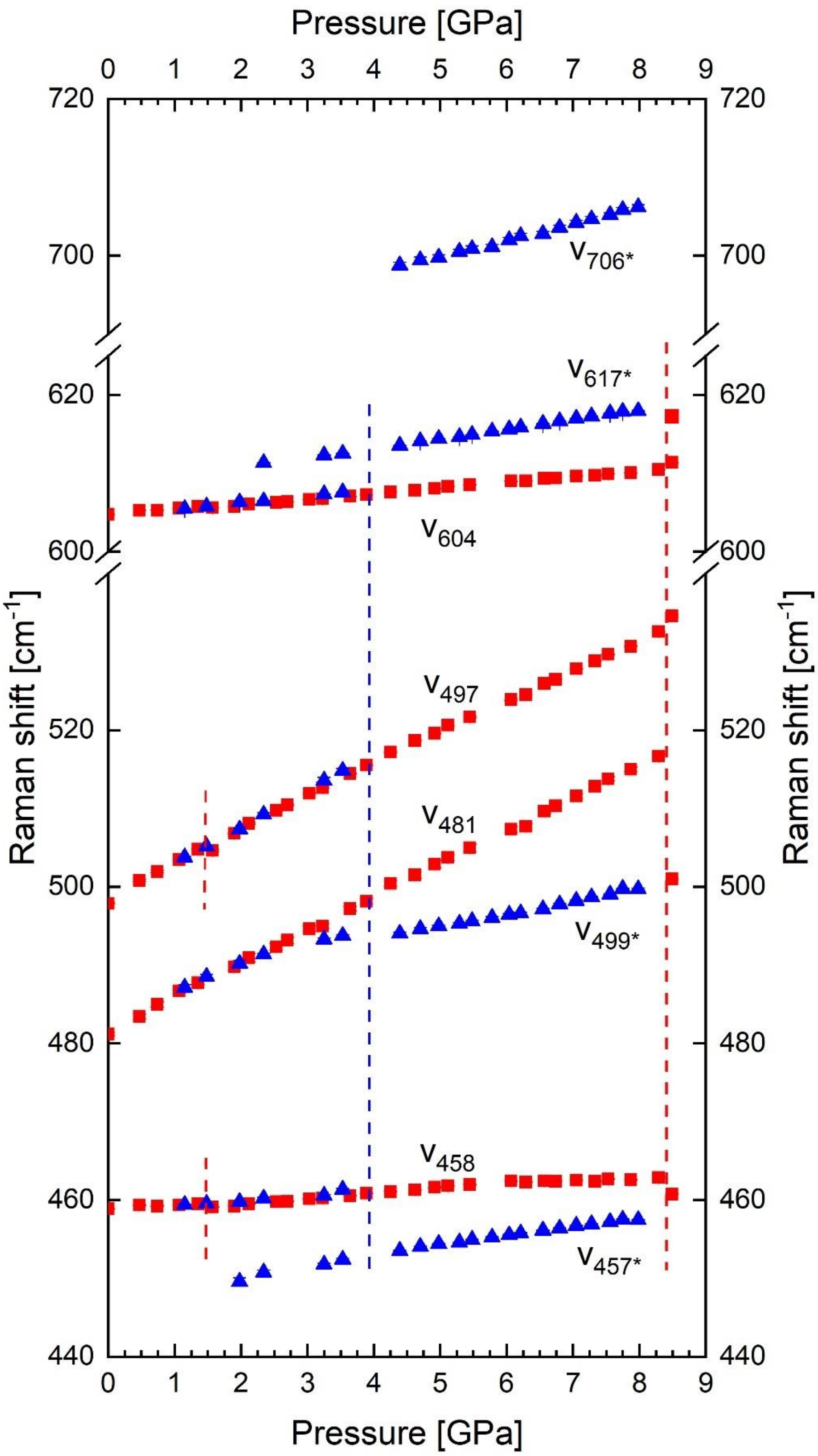

Figure 15: The evolution of the peak positions as a function of P during the compression series (red squares) and decompression series (blue triangles) of crystal 1. Vertical error bars represent the standard deviation of the exact peak position, while horizontal error bars represent the standard deviation of pressure. The red dotted line represents the P_c for a phase transition during the compression series, the blue dotted line represents the P_c during the decompression series.

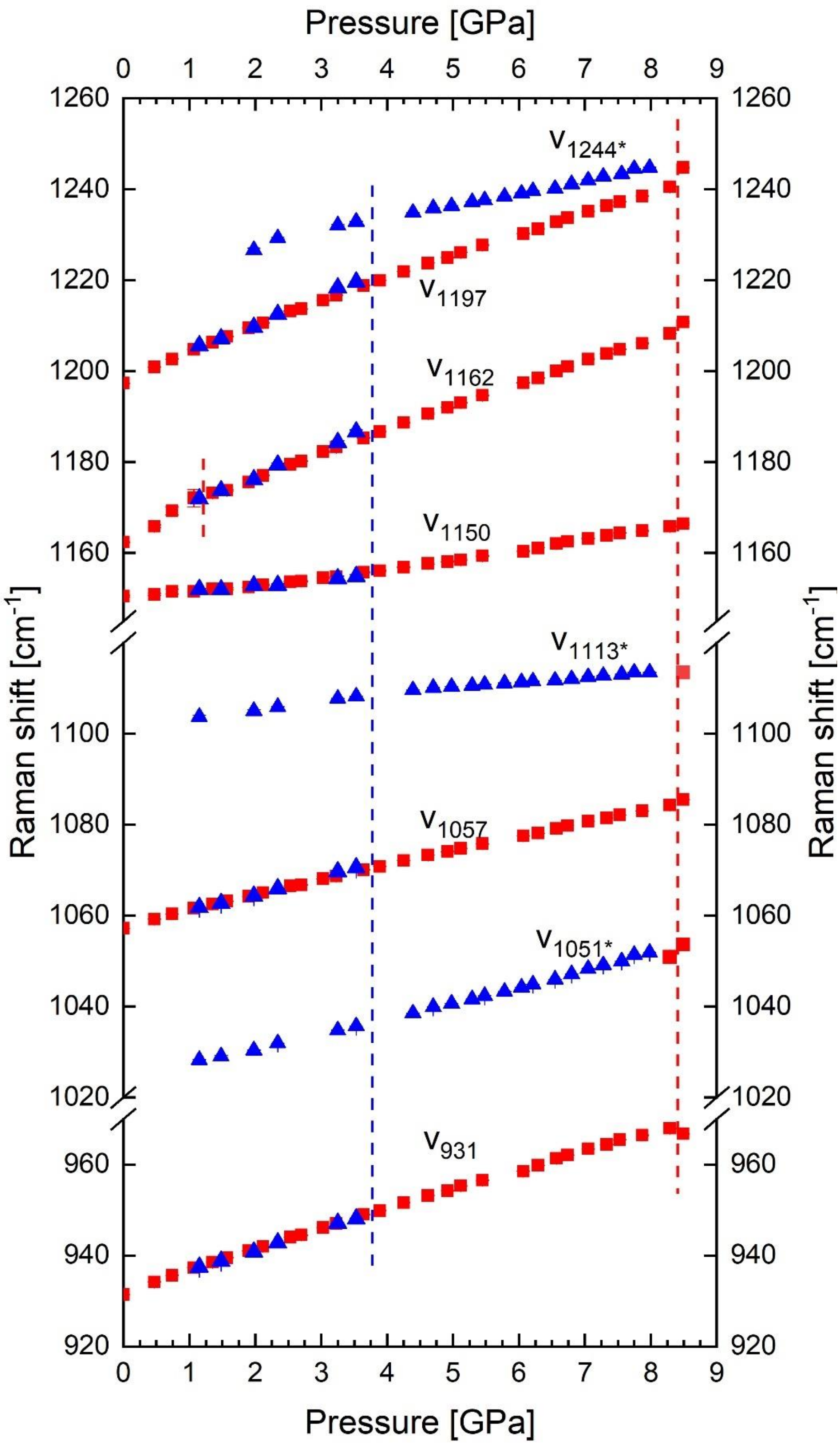

Figure 16: The evolution of the peak positions as a function of P during the compression series (red squares) and decompression series (blue triangles) of crystal 1. Vertical error bars represent the standard deviation of the exact peak position, while horizontal error bars represent the standard deviation of pressure. The red dotted line represents the P_c for a phase transition during the compression series, the blue dotted line represents the P_c during the decompression series.

For crystal 1 the Raman spectra and the associated peak position data (figures 11 – 16) show distinct changes in the high-pressure region. Between 8.29 GPa and 8.49 GPa a first order phase transition occurs. No direct references had been found to compare these results, but Ende et al. (2020) described a second phase transition on nickel sulphate monohydrate at approximately 6.5 GPa. The Raman bands at 107, 119, 188, 458, 481, 604, 931, 1057, 1150, 1162 and 1197 cm^{-1} show typical behaviour of a first order transition, by fully disappearing due to increasing hydrostatic pressure after the sample has been kept at 8 GPa for one day and their reappearance only after already decreased the pressure back to 3.53 GPa. This depicts as a large hysteresis over about 4.5 GPa, which confirms, what has been observed during X-ray diffraction (section 3.1). The Raman bands at 230*, 288*, 457*, 499*, 617*, 706*, 1050, 1113* and 1244* cm^{-1} appeared after the transformation pressure had been reached. The data also show that the phase transition does not occur spontaneously, when the transformation pressure is reached. Several Raman bands suggest a coexistence of the high-pressure and the low-pressure phase, for example the Raman bands v_{1057}, as part of the monoclinic domain, and v_{1051*}, as a part of the triclinic domain. v_{1051*} already began to appear at 8.29 GPa during the compression series, while v_{1057} did not disappear until the cell was kept at about 8 GPa for one day. The same applies for the decompression series, only now the coexistence of both phases occurs from 4.39 GPa to 1.15 GPa.

As known from the crystal structure measurements (personal communication Ende) another phase transition is to be expected, but unfortunately no distinct evidence for a phase transition at low pressure could be found. Although some Raman bands may potentially indicate a transition between 1.35 GPa and 1.57 GPa. Pistorius (1961) measured a phase transition at 2.97GPa, but at 500°C. Ende et al. (2020) described a transition on nickel sulphate monohydrate at 2.47 GPa. v_{107} and v_{119} start with almost equal intensities, but at 1.57 GPa v_{119} had suddenly decreased to about one fifth of the intensity of v_{107}. The same happens to v_{481} and v_{497}. The intensity of v_{481} is at first almost at the same hight as the intensity of v_{497} and drops to about half the hight of v_{497}. v_{580} and v_{1244} also receive a decrease in intensity in proportion to neighbouring bands. Looking at the peak positions of crystal 1 v_{268}, v_{497} and v_{1162} show a small bend in their slopes at 1.35 GPa.

For crystal 1 the average blueshifts (Δv/Δp) for each Raman band over 400cm^{-1} range from 0.18 to 5.59 cm^{-1} GPa^{-1}. Raman bands beneath 400 cm^{-1} show a range from 1.54 to 7.26 cm^{-1}. Due to the lack of literature concerning high-pressure experiments with anhydrous copper sulphate, it was not possible to compare the values directly. Ende et al. (2020) described the blueshift of nickel sulphate monohydrate having ranging values between 2.42 and 7.45 cm^{-1} GPa^{-1} and Meusburger et al. (2020) described magnesium sulphate monohydrate ranging between 2.3 and 5.06 cm^{-1} GPa^{-1}. Compared to the values of these studies the results are very similar, only the minimum blueshift of copper sulphate is approximately 2 cm^{-1} GPa^{-1} smaller than they are for nickel sulphate monohydrate.

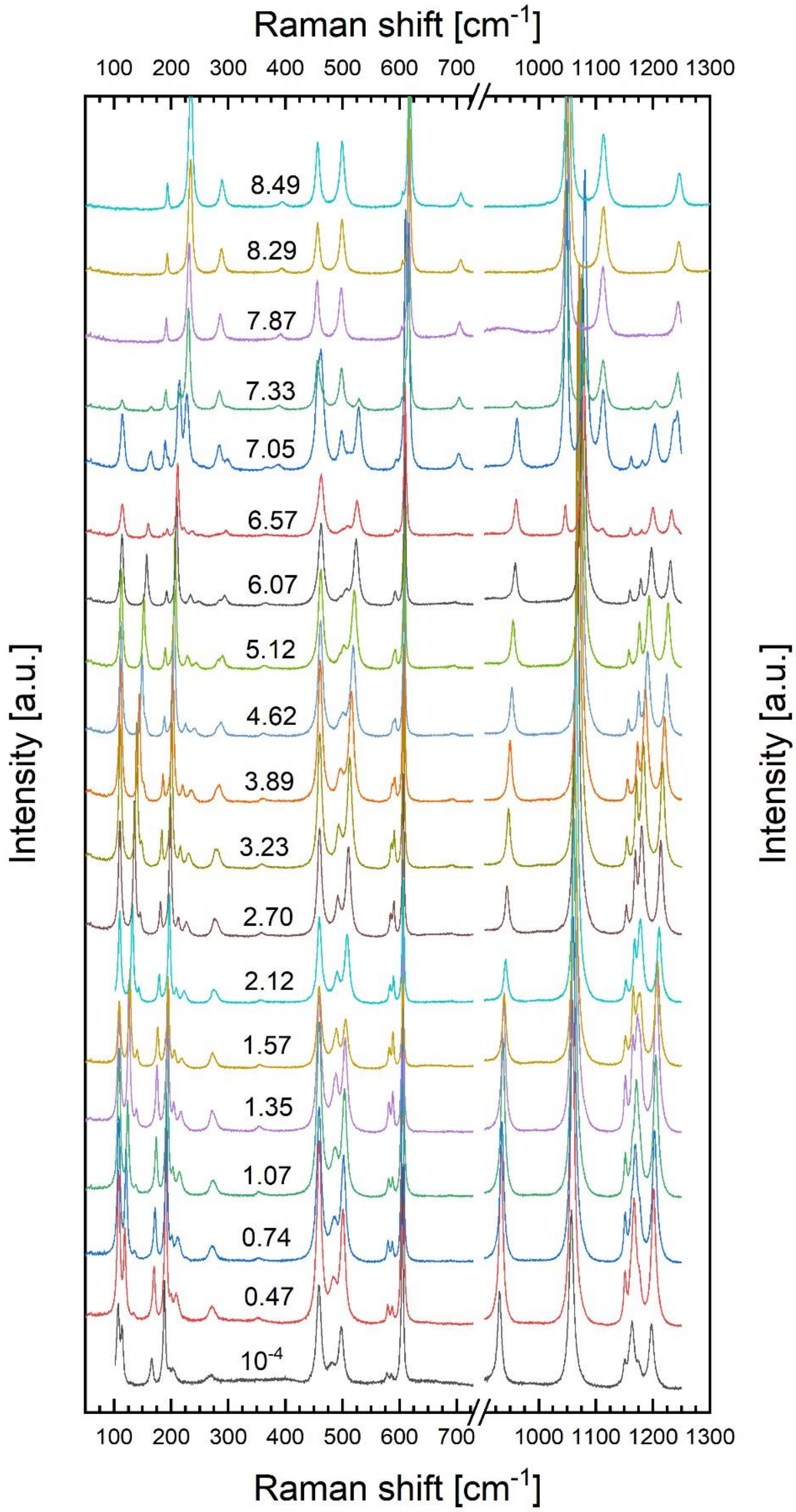

Figure 17: Stacked plot of the Raman spectra of $CuSO_4$ crystal 2, obtained during the compression series, showing changes of Raman bands under increasing hydrostatic pressure. Each spectrum is labelled with the respective pressure in GPa.

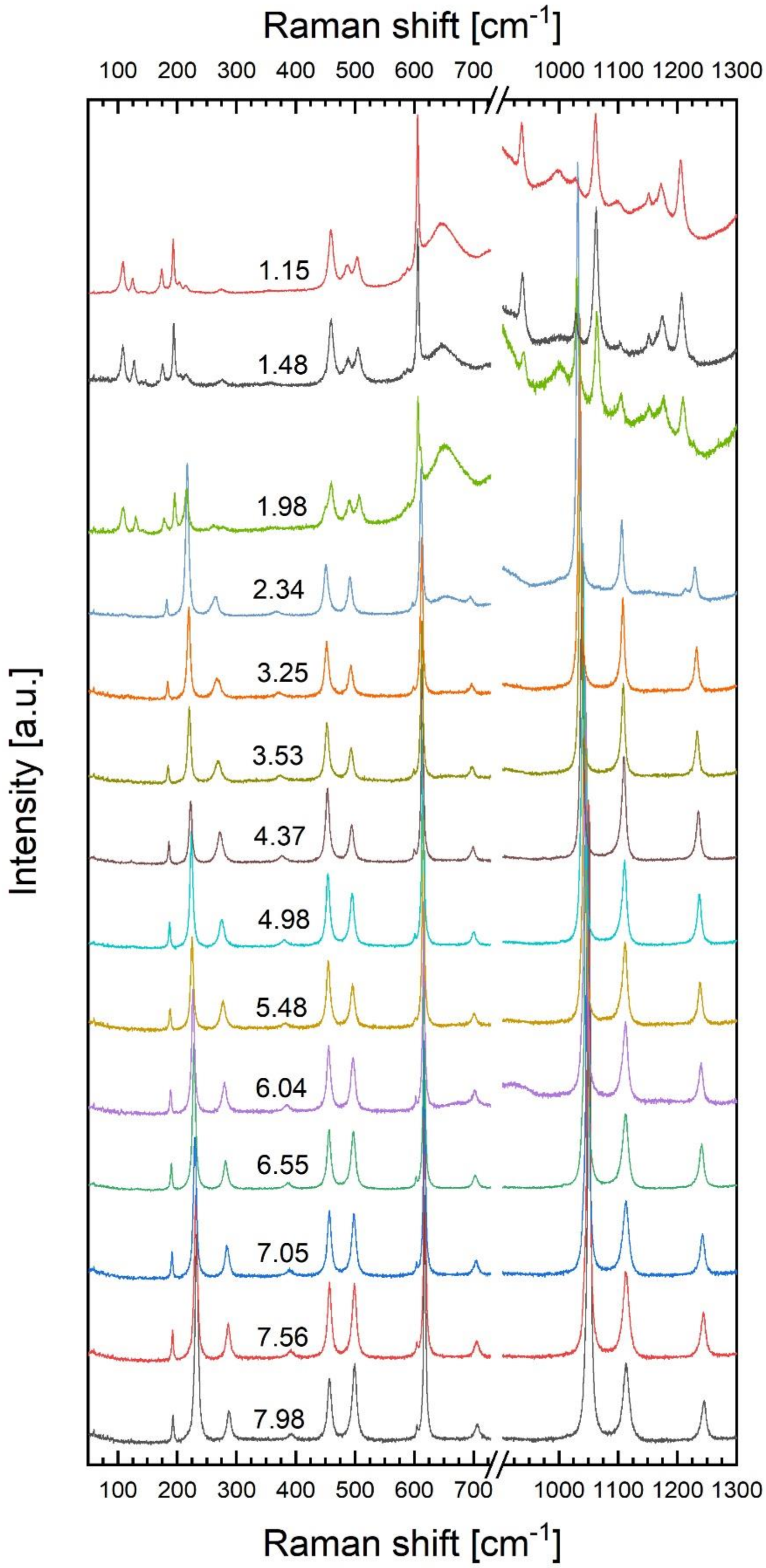

Figure 18: Stacked plot of the Raman spectra of $CuSO_4$ crystal 2, obtained during the decompression series, showing changes of Raman bands under increasing hydrostatic pressure. Each spectrum is labelled with the respective pressure in GPa.

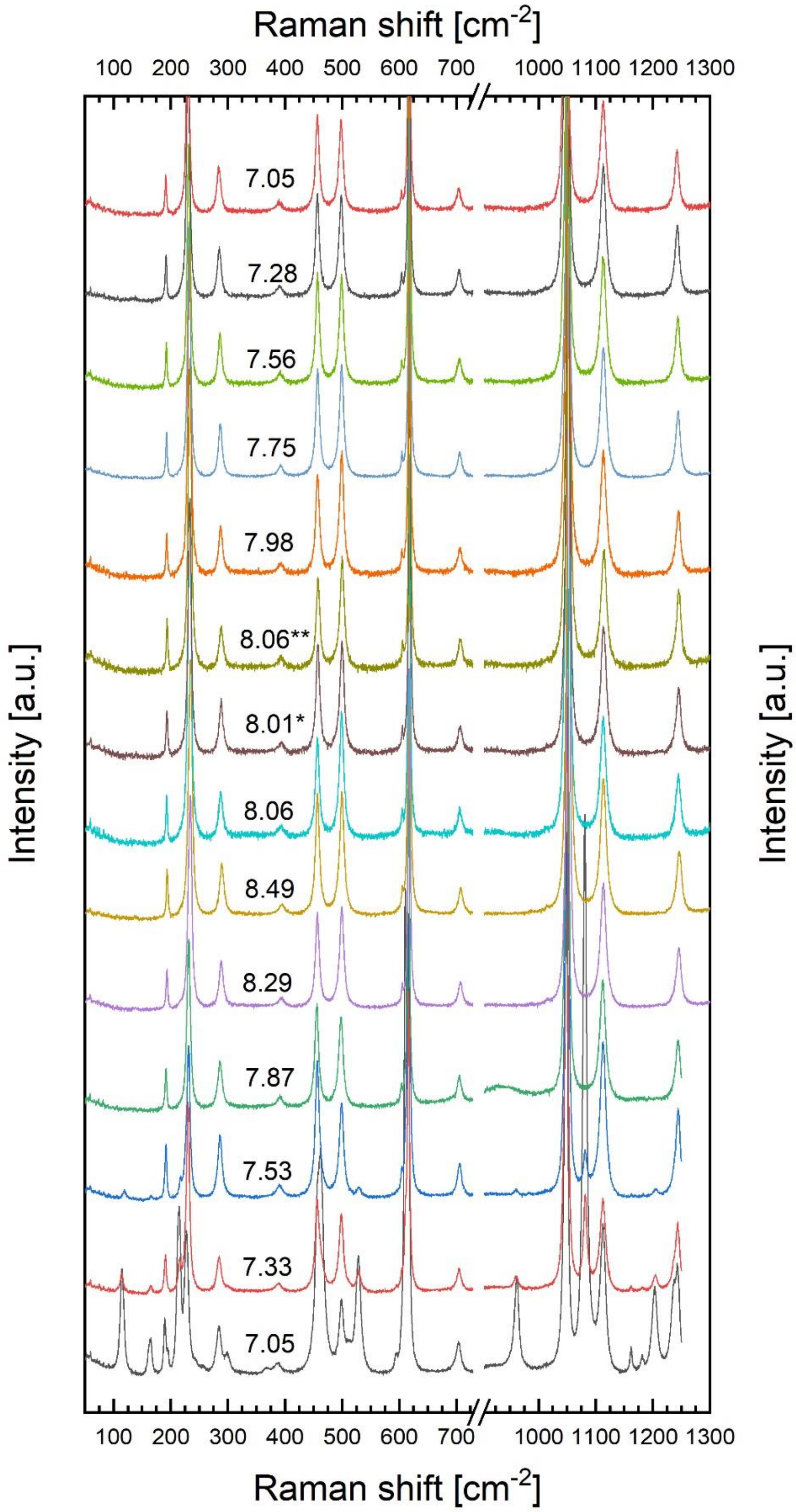

Figure 19: Stacked plot of the Raman spectra of $CuSO_4$ crystal 2, showing changes of Raman bands between the end of the compression and the start of the decompression series. Each spectrum is labelled with the respective pressure in GPa.

*: measured after 1 day; **: measured after 5 days

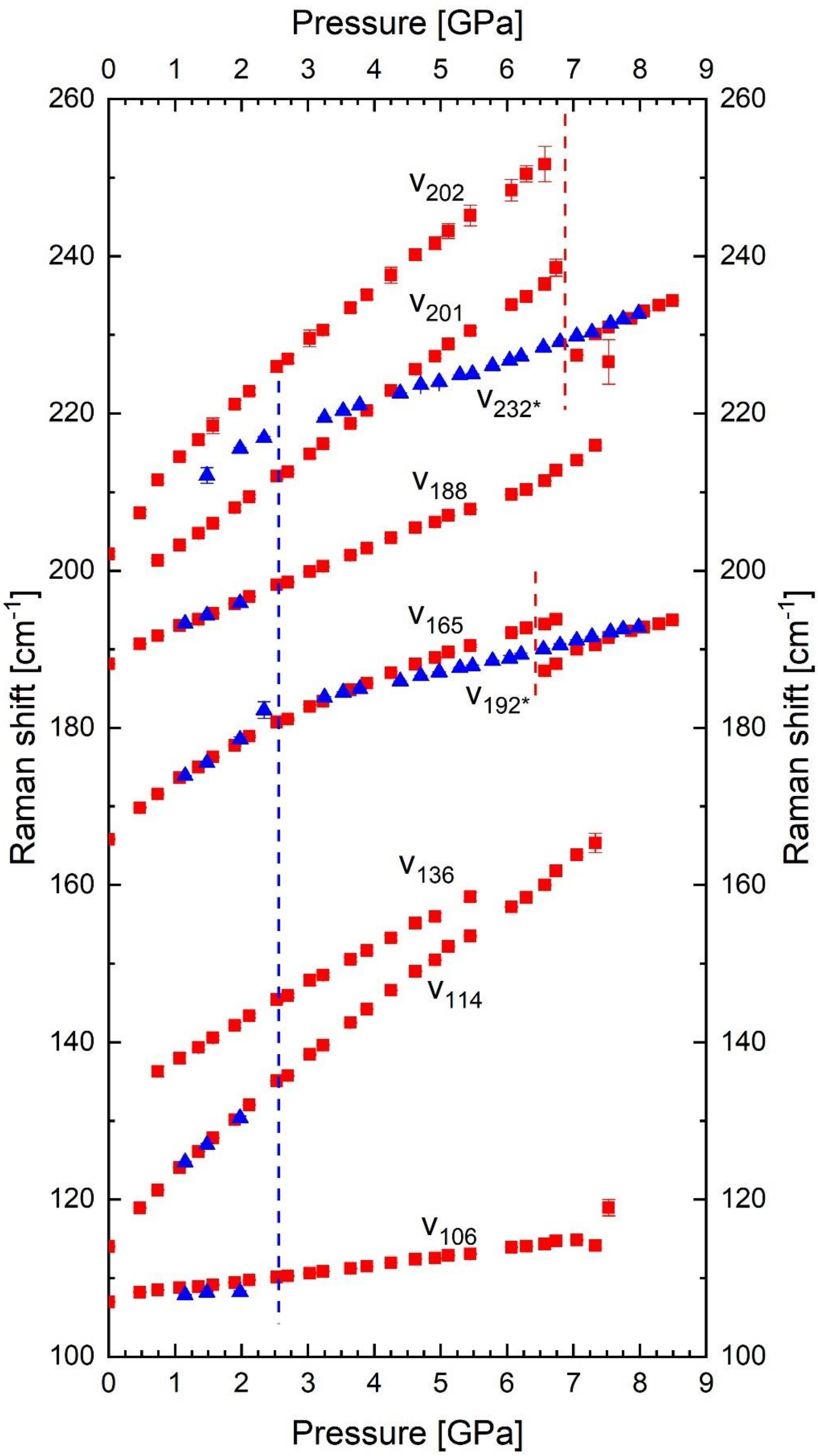

Figure 20: The evolution of the peak positions as a function of P during the compression series (red squares) and decompression series (blue triangles) of crystal 2. Vertical error bars represent the standard deviation of the exact peak position, while horizontal error bars represent the standard deviation of pressure. The red dotted line represents the P_c for a phase transition during the compression series, the blue dotted line represents the P_c during the decompression series.

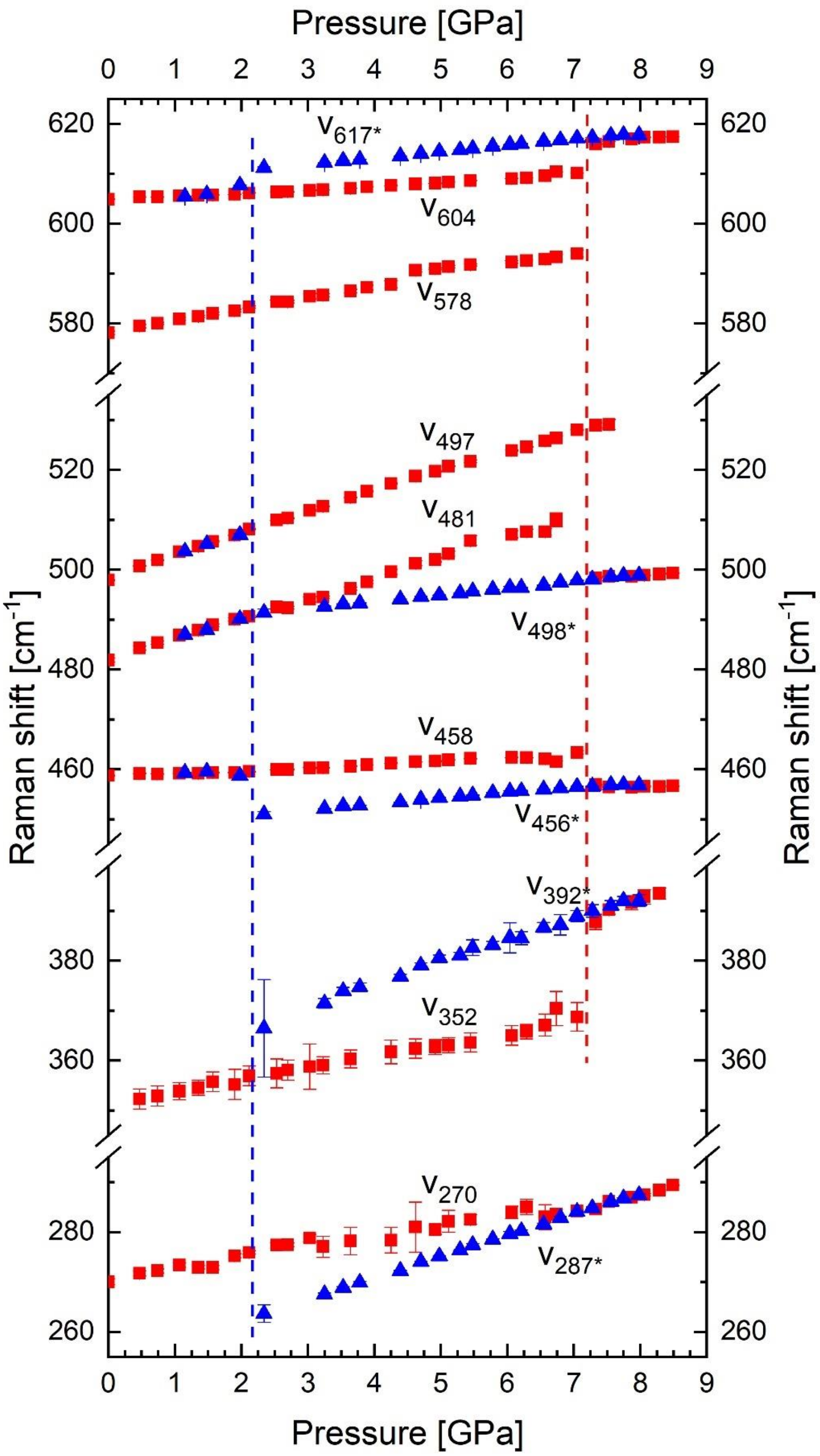

Figure 21: The evolution of the peak positions as a function of P during the compression series (red squares) and decompression series (blue triangles) of crystal 2. Vertical error bars represent the standard deviation of the exact peak position, while horizontal error bars represent the standard deviation of pressure. The red dotted line represents the P_c for a phase transition during the compression series, the blue dotted line represents the P_c during the decompression series.

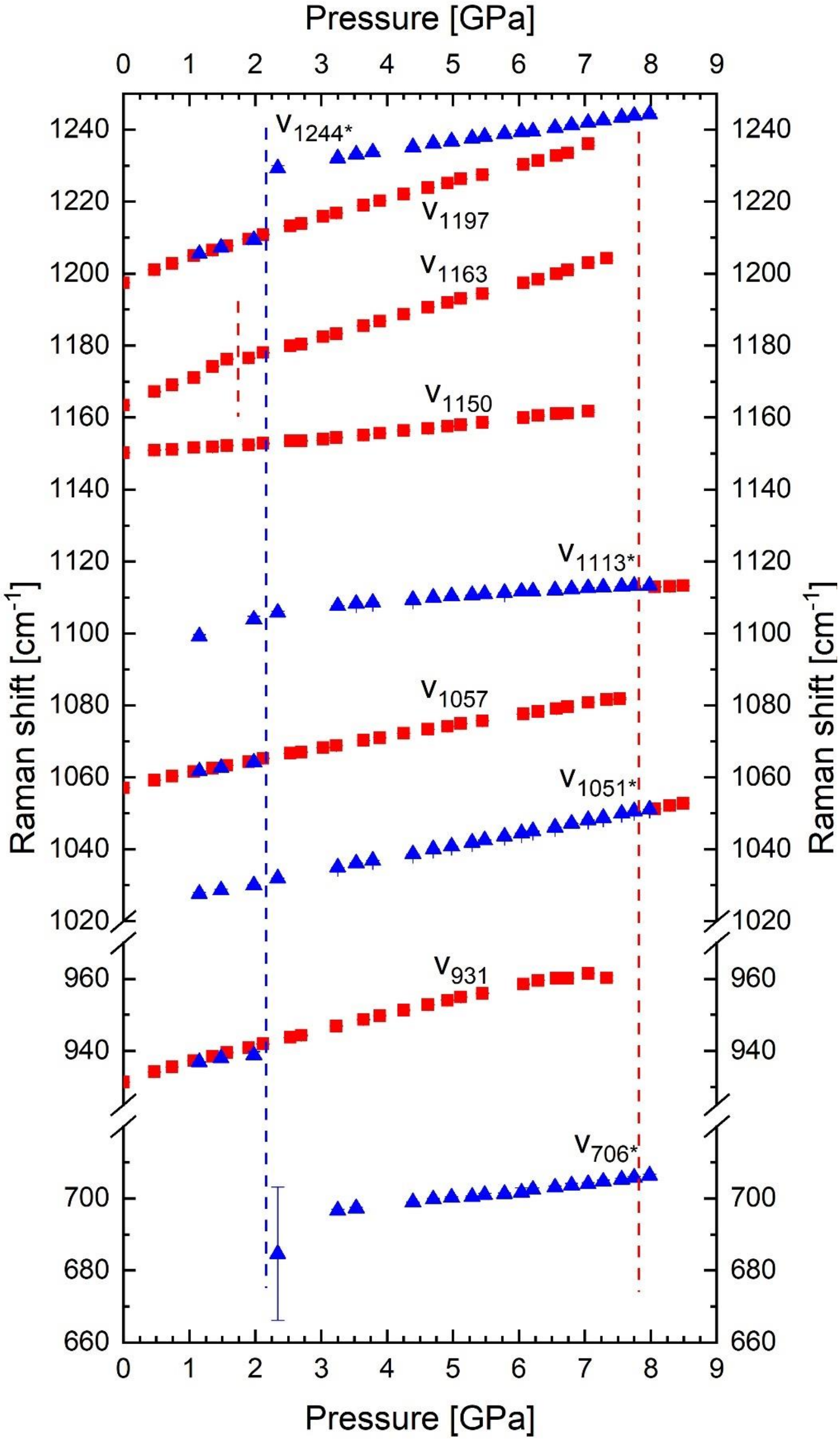

Figure 22: The evolution of the peak positions as a function of P during the compression series (red squares) and decompression series (blue triangles) of crystal 2. Vertical error bars represent the standard deviation of the exact peak position, while horizontal error bars represent the standard deviation of pressure. The red dotted line represents the P_c for a phase transition during the compression series, the blue dotted line represents the P_c during the decompression series.

Crystal 2 shows a similar behaviour to crystal 1 concerning the monoclinic-to-triclinic phase transition. For this crystal the phase transition starts at around 7.05 GPa. Crystal 2 was therefore closest to the results of approximately 6.5 GPa which Ende et al. (2020) measured on nickel sulphate monohydrate. The Raman bands at 106, 114, 188, 497, 931, 1057, 1150, 1163 and 1197 cm^{-1} start to disappear at about 7.33 GPa during compression and reappear at about 1.98 GPa. This again leads to a large hysteresis, in this case of approximately 5.0 GPa. crystal 2 also shows the coexistence of the high-pressure and the low-pressure phases, for example v_{192*} appears at 6.57 GPa next to v_{165}, which on the other hand disappears at 7.05 GPa. The coexistence can be observed during the decompression series too. V_{1051*} as well as v_{1113}, which can be assigned to the high-pressure phase, are both still visible in the last Raman spectrum of the decompression series of crystal 2 at 1.15 GPa, while the low-pressure phase Raman bands v_{931} and v_{1057} reappear already at 1.98 GPa. This observation implies that crystal 2 had not enough time to fully complete its phase transition back to its monoclinic phase.

Regarding the orthorhombic-to-monoclinic phase transition in the low-pressure region, crystal 2 shows no evidence of any phase transition.

Crystal 2 shows blueshift values similar to crystal 1. Raman bands above 400 cm^{-1} range between 0.53 and 5.40 cm^{-1} GPa^{-1} and Raman bands below 400 cm^{-1} range between 1.52 and 7.41 cm^{-1} GPa^{-1}, which again roughly coincide with the average values of Ende et al. (2020) for nickel sulphate monohydrate and Meusburger et al. (2020) for magnesium sulphate monohydrate.

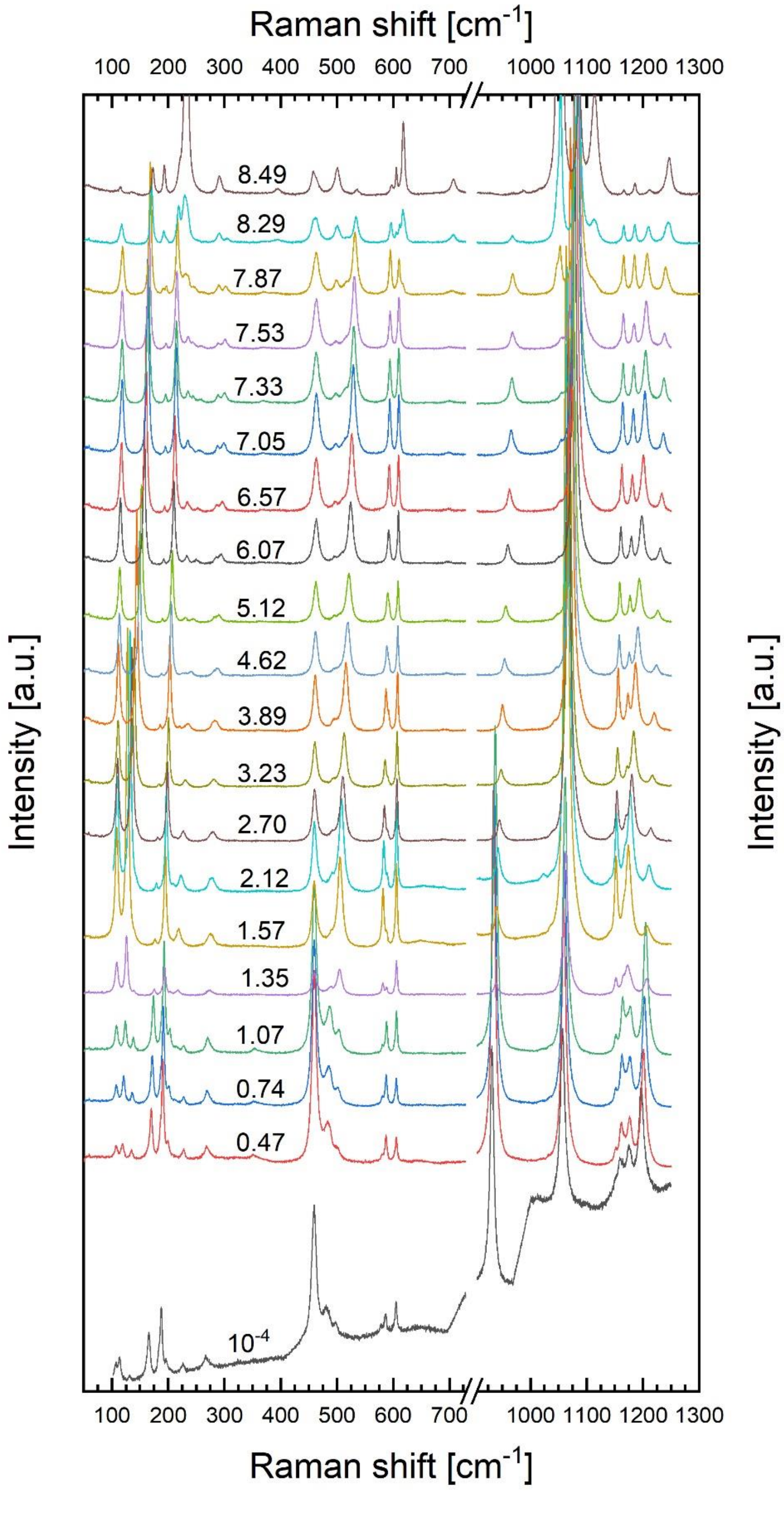

Figure 23: Stacked plot of the Raman spectra of $CuSO_4$ crystal 3, obtained during the compression series, showing changes of Raman bands under increasing hydrostatic pressure. Each spectrum is labelled with the respective pressure in GPa.

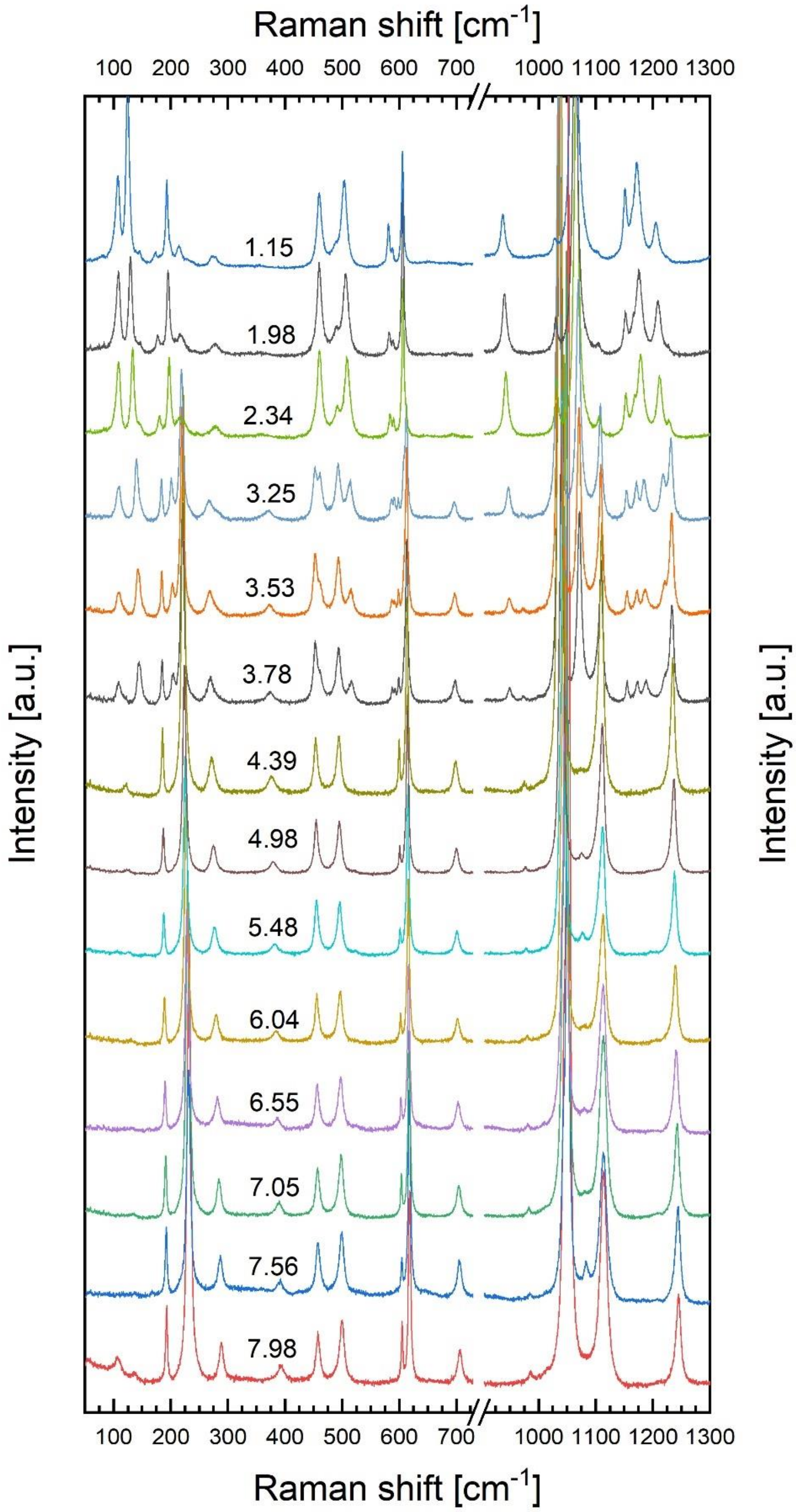

Figure 24: Stacked plot of the Raman spectra of $CuSO_4$ crystal 3, obtained during the compression series, showing changes of Raman bands under increasing hydrostatic pressure. Each spectrum is labelled with the respective pressure in GPa.

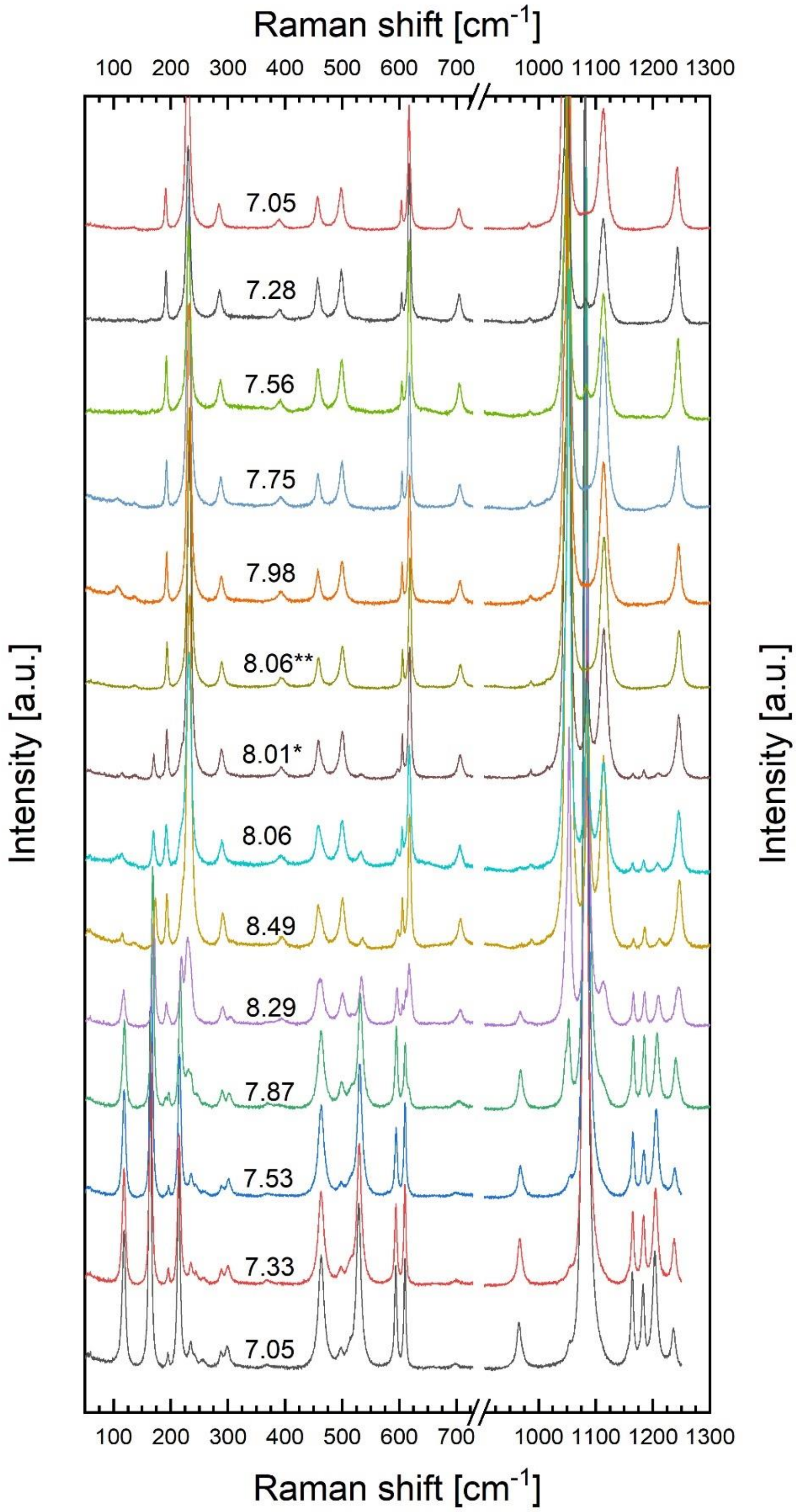

Figure 25: Stacked plot of the Raman spectra of $CuSO_4$ crystal 3, showing changes of Raman bands between the end of the compression and the start of the decompression series. Each spectrum is labelled with the respective pressure in GPa.

*: measured after 1 day; **: measured after 5 days

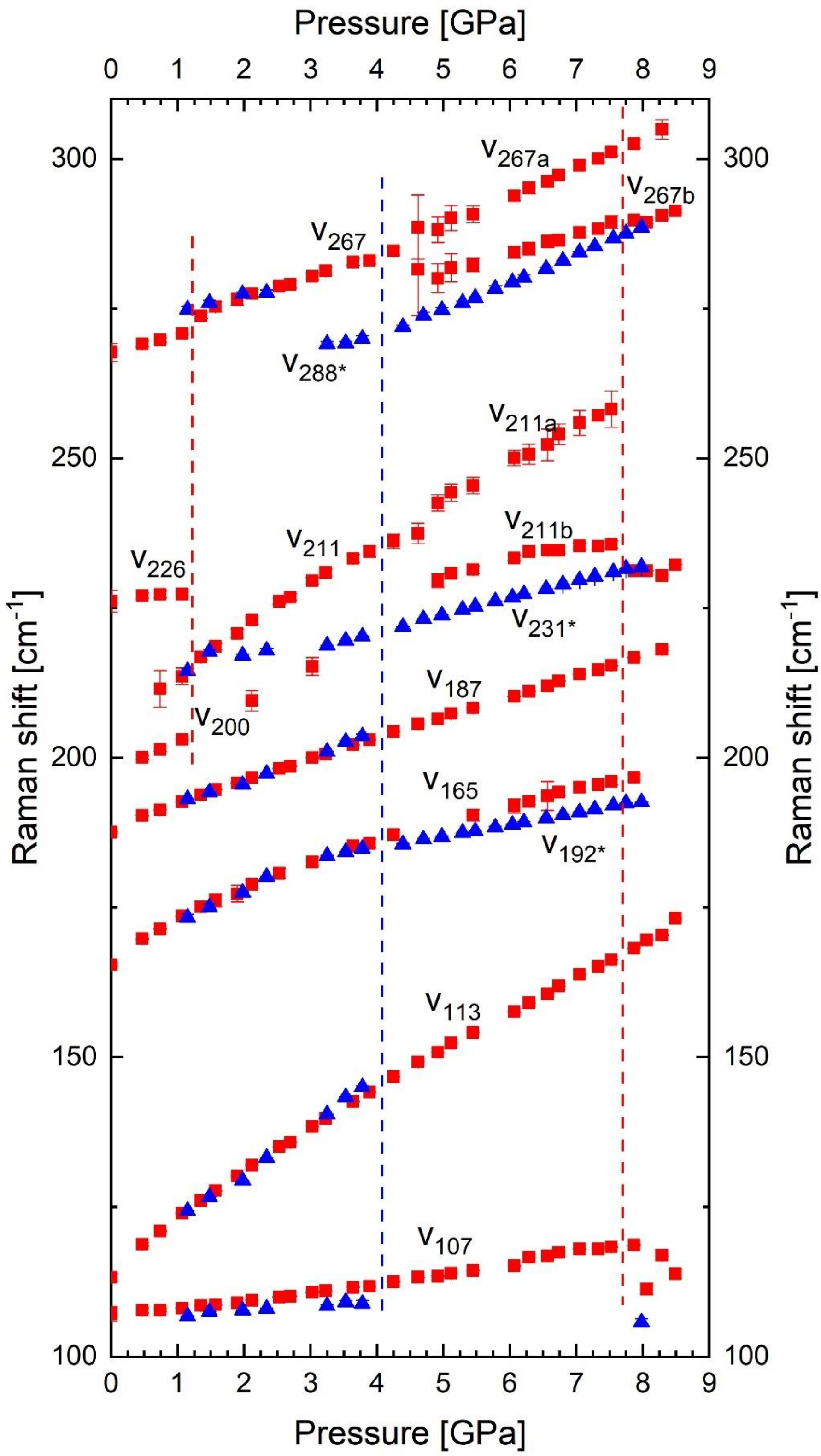

Figure 26: The evolution of the peak positions as a function of P during the compression series (squares) and decompression series (triangles) of crystal 3. Vertical error bars represent the standard deviation of the exact peak position, while horizontal error bars represent the standard deviation of pressure. The red dotted line represents the P_c for a phase transition during the compression series, the blue dotted line represents the P_c during the decompression series.

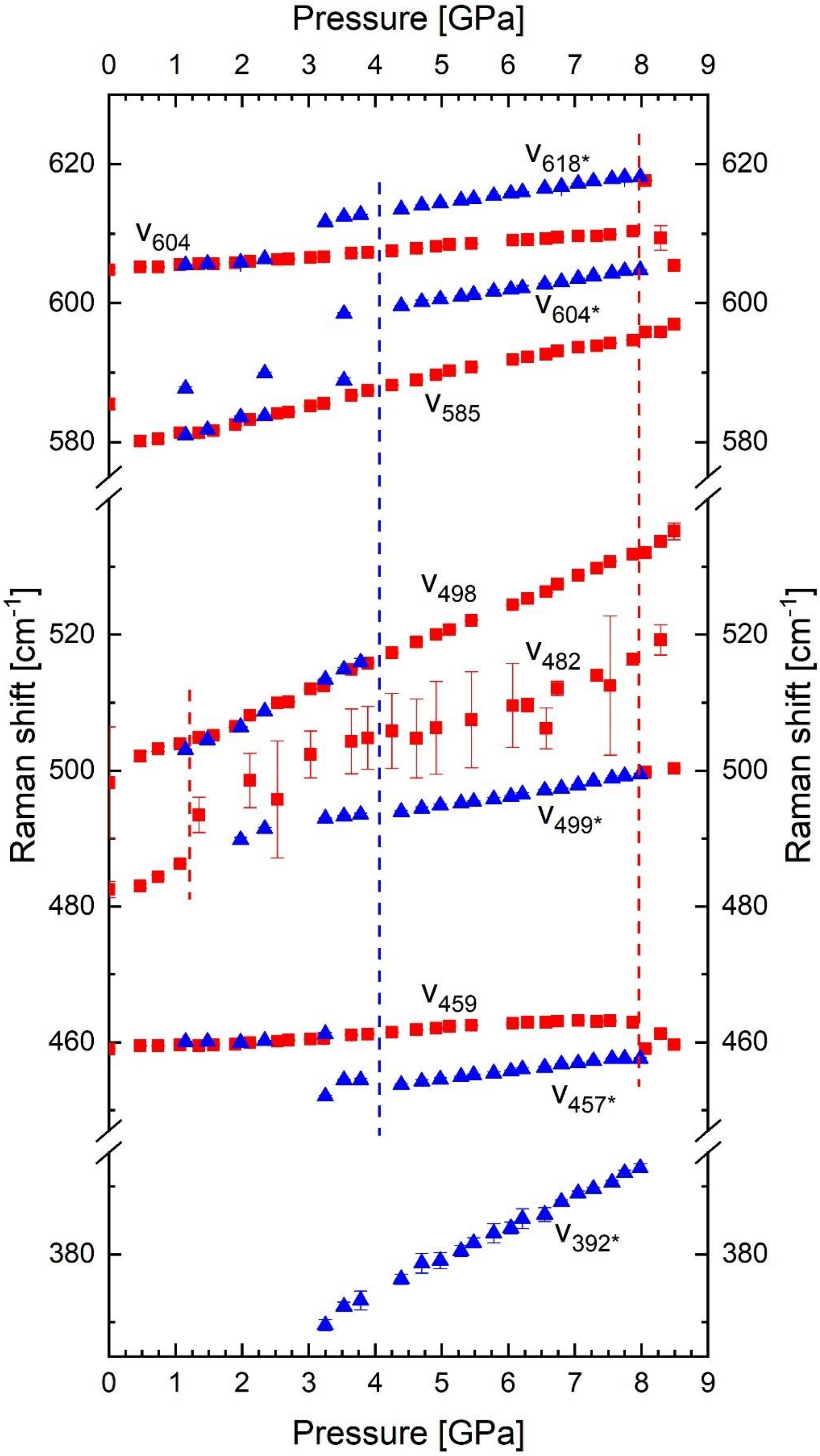

Figure 27: The evolution of the peak positions as a function of P during the compression series (red squares) and decompression series (blue triangles) of crystal 3. Vertical error bars represent the standard deviation of the exact peak position, while horizontal error bars represent the standard deviation of pressure. The red dotted line represents the P_c for a phase transition during the compression series, the blue dotted line represents the P_c during the decompression series.

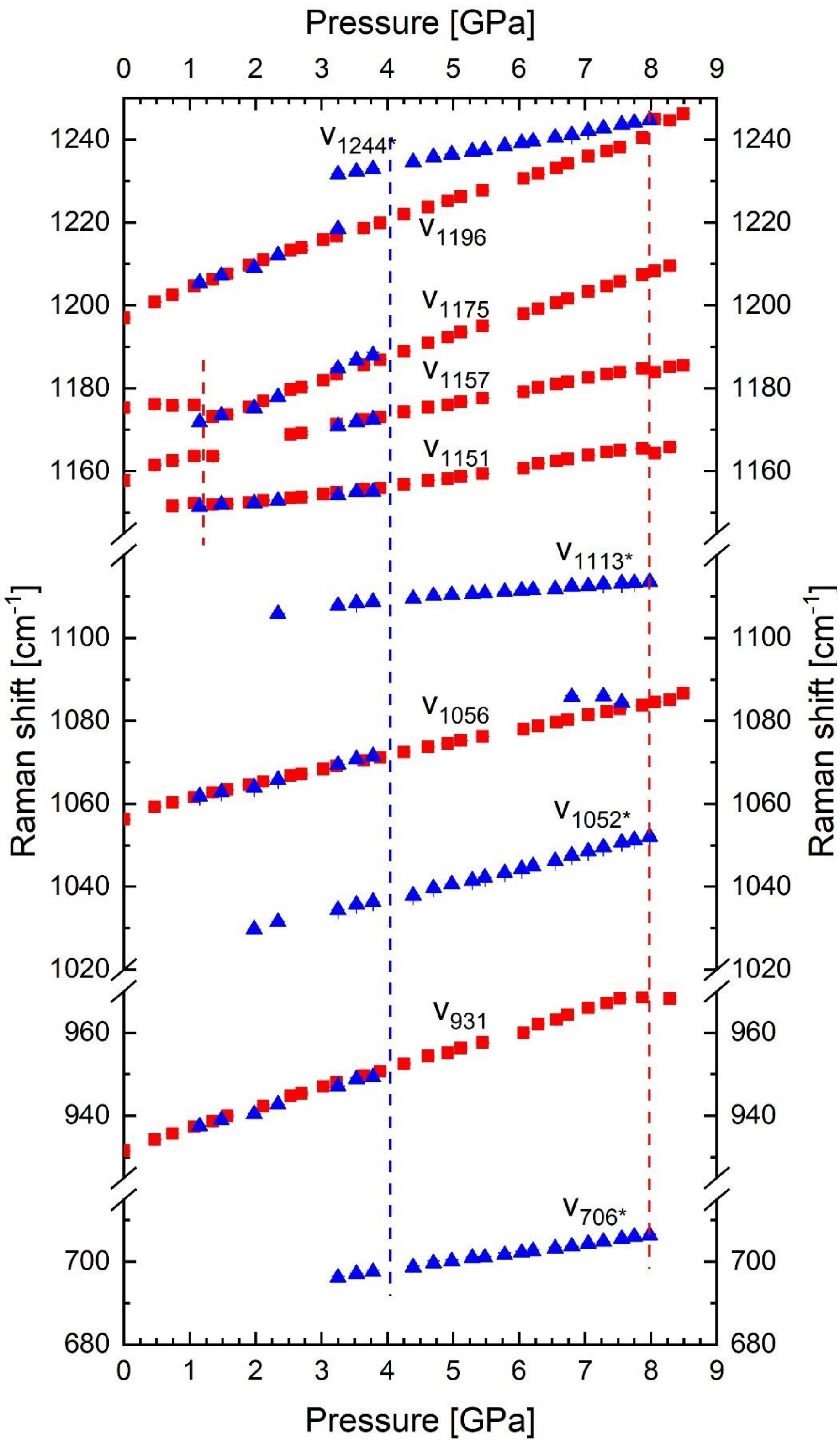

Figure 28: The evolution of the peak positions as a function of P during the compression series (red squares) and decompression series (blue triangles) of crystal 3. Vertical error bars represent the standard deviation of the exact peak position, while horizontal error bars represent the standard deviation of pressure. The red dotted line represents the P_c for a phase transition during the compression series, the blue dotted line represents the P_c during the decompression series.

Crystal 3 starts to transform at about 7.87 GPa during the compression series and at 3.78 GPa during decompression. As in the case of crystal 1 and crystal 2, crystal 3 also shows a hysteresis of approximately 5.0GPa. figures 26, 27 and 28 show, that again several bands start to disappear at 7.87 GPa and reappear at 3.78 GPa, as well as that the coexistence of the high-pressure phase and the low-pressure phase is visible in the decompression series. For example, v_{931} and v_{706*} coexist from 3.78 GPa to 3.25 GPa. During the compression series both phases begin to coexist at about 7.87 GPa and like for crystal 1 it took one day at approximately 8 GPa to fully transform into the high-pressure phase, using the example of v_{498}, which, as figure 21 shows, has almost disappeared after one day.

The Raman data of crystal 3 yield potential evidence for the first, low-pressure phase transition. Between 1.35 GPa and 1.57 GPa during the compression series the amplitude of the Raman band v_{498} strongly increases in comparison to v_{459} and the amplitudes of the Raman bands v_{931} and v_{1196} strongly decrease compared to the bands between 1150cm^{-1} and 1180cm^{-1} (see figure 23).

Crystal 3 shows blueshift values similar to crystal 1 and 2. Raman bands above 400 cm^{-1} range between 0.56 and 5.66 cm^{-1} GPa^{-1} and Raman bands below 400 cm^{-1} range between 0.76 and 6.88 cm^{-1} GPa^{-1}, which again roughly coincide with the average values of Ende et al. (2020) for nickel sulphate monohydrate and Meusburger et al. (2020) for magnesium sulphate monohydrate.

4. Conclusion

Despite complications concerning sample preparation, several $CuSO_4$ crystals have been successfully loaded in liquid argon and measured. Cryoloading of the ETH-type diamond anvil cell in combination with the use of a glovebox proved to be crucial for the success of this study, due to the very rapid hydration of the sample material. The most crucial step was, not to open the DAC until it was fully submerged in liquid argon in order to avoid the sample getting immersed in air at any point and air to a minimum. Both X-ray diffraction data and the Raman spectra distinctly show the occurrence of two phase transitions in the pressure region between 10^{-4} and 8.49 GPa on isothermal pressure variation at 298 K.

The first phase transition, which shows a symmetry reduction from orthorhombic Pnma to monoclinic $P2_1/c$, seems to take place somewhere between ambient pressure and 1 GPa. According to the X-ray diffraction results it appears to be a second order phase transition. The Raman spectrometry data show no distinct evidence of a phase transition in the lower pressure region1. More X-ray diffraction measurements are going to be needed to determine the exact critical pressure for the first phase transition.

The second phase transition occurs between 8.29 GPa and 8.49 GPa (crystal 1), 7.05 GPa and 7.33 GPa (crystal 2) and at 8.49 GPa (crystal 3) respectively during compression and between 4.39 GPa and 3.53 GPa (crystal 1), 2.34 GPa and 1.98 GPa (crystal 2), and 4.39 GPa and 3.53 GPa (crystal 3) during decompression. Due to its enormous hysteresis, it is clearly a first order phase transition, although the volume evolution does not reveal a significant volume discontinuity involved. The increase in pressure leads to a symmetry reduction from monoclinic to triclinic.

This study aims to understand phase transitions of anhydrous copper sulphate to further our knowledge of it as a possible energy storage material component. The results reveal that the first phase transition occurs even earlier than expected. This could later in the final application result in unintentional transformation of the storage material, triggered by for example an increase in gas pressure in the system. As the experiments have been conducted under isothermal conditions, it should not be neglected, that in the final application the influence of temperature could also have an impact on when the phase transitions occur.

5. References

Allan D. R.,Miletich R. and Angel R. J. (1996): A diamond-anvil cell for single-crystal x-ray diffraction studies to pressures in excess of 10 GPa. In: Rev. Sci. Instrum. (67), S. 840.

Angel, R. J., Allan, D. R., Miletich, R., & Finger, L. W. (1997). The use of quartz as an internal pressure standard in high-pressure crystallography. *Journal of Applied Crystallography*, *30*(4), 461-466.

Angel R. J. (2000): Equations of State. In: Reviews in Mineralogy and Geochemistry (41), S. 35–59

Angel R. J. and Finger L. W. (2011): SINGLE: a program to control single-crystal diffractometers. In: J. Appl. Cryst. (44), S. 247–251.

Benedict, S. R. (1909). A reagent for the detection of reducing sugars. *Journal of Biological Chemistry*, *5*(5), 485-487.

Birch F. (1947): Finite Elastic Strain of Cubic Crystals. In: Phys. Rev. (71), S. 809.

Comodi, P., Fastelli, M., Maturilli, A., Balic-Zunic, T., & Zucchini, A. (2021). Emissivity and reflectance spectra at different temperatures of hydrated and anhydrous sulphates: A contribution to investigate the composition and dynamic of icy planetary bodies. *Icarus*, *355*, 114132.

Cot-Gores, J., Castell, A., & Cabeza, L. F. (2012). Thermochemical energy storage and conversion: A-state-of-the-art review of the experimental research under practical conditions. *Renewable and Sustainable Energy Reviews*, *16*(7), 5207-5224.

Dunitz, J. D., & Pauling, P. (1965). Polymorphism in anhydrous cobalt sulphate. *Acta Crystallographica*, *18*(4), 737-740.

Ende, M., Kirkkala, T., Loitzenbauer, M., Talla, D., Wildner, M., & Miletich, R. (2020). High-Pressure Behavior of Nickel Sulfate Monohydrate: Isothermal Compressibility, Structural Polymorphism, and Transition Pathway. *Inorganic chemistry*, *59*(9), 6255-6266.

Fu, X., Yang, G., Sun, J., & Zhou, J. (2012). Vibrational spectra of copper sulfate hydrates investigated with low-temperature Raman spectroscopy and Terahertz time domain spectroscopy. *The Journal of Physical Chemistry A*, *116*(27), 7314-7318.

Gibson, C. E. (1972). The algicidal effect of copper on a green and a blue-green alga and some ecological implications. *Journal of applied ecology*, 513-518.

Gonzalez-Platas J., Alvaro M., Nestola F. and Angel R. J. (2016): EosFit7-GUI: a new graphical user interface for equation of state calculations, analyses and teaching. In: J. Appl. Cryst. (49), S. 1377–1382.

Hoffman, R. V., Bishop, R. D., Fitch, P. M., & Hardenstein, R. (1980). Anhydrous copper (II) sulfate: an efficient catalyst for the liquid-phase dehydration of alcohols. *The Journal of Organic Chemistry*, *45*(5), 917-919.

Johnson, G. F. (1935). The early history of copper fungicides. *Agricultural History*, *9*(2), 67-79.

Katsura, T., & Tange, Y. (2019). A Simple Derivation of the Birch–Murnaghan Equations of State (EOSs) and Comparison with EOSs Derived from Other Definitions of Finite Strain. *Minerals*, *9*(12), 745.

King Jr. H. E. and Finger L. W. (1979): Diffracted Beam Crystal Centering and Its Application to High-Pressure Crystallography. In: J. Appl. Cryst. (12), S. 374–378.

Klotz, S., Paumier, L., Le March, G., & Munsch, P. (2009). The effect of temperature on the hydrostatic limit of 4: 1 methanol–ethanol under pressure. *High Pressure Research*, *29*(4), 649-652.

Kokkoros, P. A., & Rentzeperis, P. J. (1958). The crystal structure of the anhydrous sulphates of copper and zinc. *Acta Crystallographica*, *11*(5), 361-364.

Lele, A. F. (2016). State-of-Art of Thermochemical Heat Storage Systems. In *A Thermochemical Heat Storage System for Households* (pp. 15-58). Springer, Cham.

Mao, H. K. (1980). Design and Operation of a Diamond-Window, High-Pressure Cell for the Study of Single Crystal Samples Loaded Cryogenically. *Carnegie Inst. Washington Year Book*, *79*, 409-411.

Mao, H. K., Xu, J. A., & Bell, P. M. (1986). Calibration of the ruby pressure gauge to 800 kbar under quasi-hydrostatic conditions. *Journal of Geophysical Research: Solid Earth*, *91*(B5), 4673-4676.

Meusburger, J. M., Ende, M., Matzinger, P., Talla, D., Miletich, R., & Wildner, M. (2020). Polymorphism of Mg-monohydrate sulfate kieserite under pressure and its occurrence on giant icy Jovian satellites. *Icarus*, *336*, 113459.

Miletich R., Allan D. R. and Kuhs W. F. (2000): High-Pressure Single-Crystal Techniques. In: Reviews in Mineralogy and Geochemistry (41), S. 445–519.

Müller, D., Knoll, C., Gravogl, G., Lager, D., Welch, J. M., Eitenberger, E., ... & Weinberger, P. (2020). CuSO4/[Cu (NH3) 4] SO4-Composite Thermochemical Energy Storage Materials. *Nanomaterials*, *10*(12), 2485.

Müller, D., Knoll, C., Gravogl, G., Jordan, C., Eitenberger, E., Friedbacher, G., ... & Weinberger, P. (2021). Medium-temperature thermochemical energy storage with transition metal ammoniates–A systematic material comparison. *Applied Energy*, *285*, 116470.

Pistorius, C. W. (1961). Polymorphism in the anhydrous sulphates of Mn, Fe, Co, Ni, Cu and Zn to 140,000 bars and 750° C. *Zeitschrift für Kristallographie-Crystalline Materials*, *116*(3-6), 220-250.

Prieto, C., Cooper, P., Fernández, A. I., & Cabeza, L. F. (2016). Review of technology: thermochemical energy storage for concentrated solar power plants. *Renewable and Sustainable Energy Reviews*, *60*, 909-929.

Scacchi A. (1873) Nuove specie di solfati di rame. Att Accad Sci Fis Mat Napoli 5: Nr 3, 22-29

Scheidl. K. S., Kurnosov A., Trots D. M., Ballaran T. B., Angel R. J., Miletich R. (2016): Extending the single-crystal quartz pressure gauge up to hydrostatic pressure of 19 GPa. In: J. Appl. Cryst. (49), S. 2129–2137.

Stoe & Cie (2002). X-Area. Stoe & Cie, Darmstadt, Germany

Sushanthi L. C.; Sherlin, H. J., Jayaraj, G., Don, K. R., & Santhanam, A. (2020). Efficacy of Anhydrous Copper Sulphate as a Solid Dehydrant in Tissue Processing Procedure. *Journal of Evolution of Medical and Dental Sciences*, *9*(40), 3004-3009.

Vaniman, D. T., Bish, D. L., Chipera, S. J., Fialips, C. I., Carey, J. W., & Feldman, W. C. (2004). Magnesium sulphate salts and the history of water on Mars. *Nature*, *431*(7009), 663-665.

Wehner, H. L., Spiering, H., & Ritter, G. (1976). Polymorphism of anhydrous ferrous sulfate. *Solid State Communications*, *20*(9), 831-835.

Wildner, M., & Giester, G. (1988). Crystal structure refinements of synthetic chalcocyanite (CuSO 4) and zincosite (ZnSO 4). *Mineralogy and Petrology*, *39*(3-4), 201-209. the anhydrous sulphates of copper and zinc. *Acta Crystallographica*, *11*(5), 361-364.

6. Table of tables

7. Table of figures

8. Table of equations

9. Appendix

The following tables contain the results from peak-fitting the measured Raman data. Raman bands are named according to their respective first occurrence in either the compression or the decompression series (marked with a "*")

SE	standard error
c1, c2, c3	sample crystal 1,2 and 3
p	pressure [GPa]

	c1-compression series							
p	v107	SE	v119	SE	v165	SE	v188	SE
1Atm					165.89	0.05	188.06	0.03
0.47	107.27	0.12	119.10	0.09	169.75	0.07	190.44	0.04
0.74	107.58	0.08	121.22	0.07	171.51	0.09	191.46	0.05
1.07	108.30	0.06	123.83	0.06	173.57	0.06	192.81	0.03
1.35	108.44	0.06	126.03	0.06	175.03	0.07	193.78	0.04
1.57	108.66	0.08	127.72	0.24	176.02	0.17	194.49	0.03
1.9	109.02	0.05	130.05	0.19	177.57	0.12	195.69	0.02
2.12	109.21	0.06	131.59	0.20	178.60	0.14	196.55	0.03
2.53	109.84	0.06	134.83	0.19	180.48	0.15	198.04	0.02
2.7	110.00	0.05	135.66	0.15	180.86	0.11	198.39	0.02
3.03	110.51	0.05	138.19	0.13	182.42	0.12	199.74	0.03
3.23	110.78	0.05	139.66	0.16	183.03	0.11	200.36	0.03
3.64	111.79	0.04	142.34	0.15	184.53	0.12	201.93	0.02
3.89	111.65	0.05	144.00	0.18	185.38	0.11	202.72	0.03
4.25	112.48	0.05	146.51	0.15	186.66	0.12	204.06	0.03
4.62	112.80	0.05	148.82	0.14	187.75	0.12	205.31	0.03
4.92	113.19	0.05	150.33	0.12	188.55	0.16	206.22	0.04
5.12	113.65	0.05	151.98	0.14	189.29	0.12	206.95	0.03
5.45	113.80	0.08	153.76	0.20	189.98	0.15	207.90	0.04
6.07	114.41	0.06	157.21	0.18	191.75	0.15	209.87	0.03
6.29	114.84	0.08	158.32	0.15	192.24	0.16	210.47	0.04
6.57	115.98	0.04	160.18	0.14	193.12	0.10	211.49	0.03
6.74	116.13	0.05	161.42	0.14	193.66	0.13	212.21	0.03
7.05	116.64	0.04	163.06	0.10	194.43	0.10	213.25	0.03
7.33	116.73	0.04	164.39	0.09	195.13	0.10	214.06	0.03
7.53	117.16	0.04	165.39	0.12	195.67	0.10	214.72	0.03
7.87	117.33	0.05	166.82	0.11	196.40	0.12	215.59	0.03
8.29	117.61	0.04	168.95	0.10	197.49	0.10	217.07	0.02
8.49	119.66	0.14	172.62	0.36	198.12	0.33	220.48	0.06
8.06	119.16	0.46	171.22	0.89	191.74	0.25	220.33	0.16

	c1-compression series							
p	v199	SE	v268	SE	v458	SE	v481	SE
1Atm			268.68	0.34	458.88	0.04	481.20	0.19
0.47	199.64	0.33	270.48	0.63	459.34	0.06	483.44	0.32
0.74	201.29	0.30	271.42	0.55	459.24	0.07	484.99	0.32
1.07	202.94	0.19	272.03	0.46	459.34	0.05	486.68	0.21
1.35	204.70	0.19	272.83	0.46	459.48	0.05	487.73	0.19
1.57	205.56	0.57	275.48	1.15	459.14	0.05		
1.9	207.62	0.39	277.05	0.67	459.23	0.03	489.75	0.41
2.12	209.17	0.35	276.91	0.82	459.51	0.04	490.95	0.54
2.53	211.50	0.36	278.83	0.71	459.78	0.03	492.34	0.41
2.7	212.44	0.25	279.30	0.61	459.85	0.03	493.16	0.41
3.03	214.78	0.31	280.49	0.59	460.18	0.04	494.66	0.36
3.23	215.86	0.27	281.17	0.57	460.28	0.04	495.00	0.32
3.64	218.64	0.25	283.25	0.50	460.55	0.03	497.21	0.30
3.89	220.25	0.29	283.60	0.59	460.86	0.04	498.17	0.35
4.25	222.59	0.32	285.98	0.56	461.09	0.04	500.41	0.37
4.62	225.03	0.33	287.29	0.64	461.32	0.04	501.50	0.44
4.92	227.08	0.43	288.35	0.56	461.62	0.06	502.91	0.46
5.12	228.49	0.31	288.46	0.65	461.84	0.05	503.72	0.39
5.45	230.22	0.41	290.33	0.78	461.99	0.06	504.95	0.51
6.07	233.93	0.30	293.14	0.49	462.46	0.05	507.33	0.38
6.29	235.47	0.41	293.51	0.71	462.30	0.07	507.71	0.35
6.57	237.63	0.26	294.98	0.50	462.46	0.05	509.68	0.32
6.74	238.57	0.36	296.34	0.55	462.38	0.05	510.33	0.27
7.05	240.99	0.30	297.58	0.45	462.53	0.05	511.58	0.29
7.33	242.44	0.28	298.59	0.44	462.41	0.05	512.83	0.26
7.53	244.39	0.29	299.89	0.42	462.66	0.05	513.80	0.26
7.87	246.57	0.46	301.05	0.59	462.59	0.06	515.01	0.30
8.29	249.47	0.36	303.47	0.34	462.89	0.03	516.68	0.24
8.49	253.91	1.03	305.38	0.94	460.76	0.06	501.00	0.16
8.06	230.12	0.16	302.70	3.20	463.39	1.04	500.00	0.26

	c1-compression series							
p	v497	SE	v604	SE	v931	SE	v1057	SE
1Atm	497.87	0.08	604.77	0.01	931.39	0.02	1057.20	0.01
0.47	500.82	0.15	605.28	0.02	934.17	0.04	1059.26	0.03
0.74	501.95	0.14	605.28	0.02	935.64	0.04	1060.37	0.02
1.07	503.47	0.11	605.55	0.02	937.33	0.03	1061.65	0.02
1.35	504.76	0.10	605.76	0.02	938.54	0.03	1062.56	0.02
1.57	504.63	0.14	605.62	0.01	939.52	0.04	1063.16	0.03
1.9	506.82	0.11	605.76	0.01	941.00	0.03	1064.25	0.02
2.12	508.12	0.13	606.09	0.01	942.01	0.03	1065.07	0.02
2.53	509.76	0.11	606.28	0.01	944.04	0.03	1066.52	0.02
2.7	510.45	0.11	606.36	0.01	944.48	0.03	1066.79	0.02
3.03	511.92	0.10	606.64	0.01	946.15	0.03	1068.11	0.02
3.23	512.63	0.09	606.75	0.01	946.99	0.03	1068.69	0.02
3.64	514.46	0.09	607.06	0.01	949.02	0.03	1070.11	0.02
3.89	515.55	0.10	607.28	0.01	949.89	0.04	1070.83	0.02
4.25	517.20	0.10	607.59	0.01	951.64	0.04	1072.10	0.02
4.62	518.64	0.10	607.85	0.01	953.20	0.04	1073.31	0.02
4.92	519.63	0.11	608.08	0.01	954.27	0.06	1074.10	0.03
5.12	520.63	0.10	608.33	0.01	955.36	0.04	1074.81	0.02
5.45	521.68	0.13	608.53	0.01	956.55	0.06	1075.79	0.03
6.07	523.91	0.12	609.00	0.01	958.54	0.05	1077.51	0.02
6.29	524.55	0.10	609.01	0.01	959.85	0.06	1078.15	0.03
6.57	525.97	0.09	609.37	0.01	961.36	0.04	1079.11	0.02
6.74	526.49	0.08	609.41	0.01	962.10	0.05	1079.78	0.02
7.05	527.86	0.06	609.66	0.01	963.44	0.04	1080.75	0.02
7.33	528.85	0.06	609.72	0.01	964.42	0.04	1081.49	0.02
7.53	529.68	0.07	609.94	0.01	965.47	0.04	1082.13	0.02
7.87	530.70	0.08	610.05	0.01	966.47	0.05	1083.00	0.02
8.29	532.58	0.05	610.47	0.01	967.98	0.04	1084.33	0.01
8.49	534.58	0.16	611.38	0.03	966.75	0.11	1085.52	0.03
8.06	533.20	0.36	615.57	0.04	964.27	0.30	1084.42	0.06

	c1-compression series							
p	v1150	SE	v1162	SE	v1197	SE		
1Atm	1150.49	0.22	1162.34	0.10	1197.32	0.04		
0.47	1150.86	0.25	1165.89	0.25	1200.90	0.04		
0.74	1151.48	0.49	1169.23	0.89	1202.65	0.04		
1.07	1151.55	0.25	1172.06	1.90	1204.78	0.03		
1.35	1152.07	0.19	1173.18	0.35	1206.32	0.03		
1.57	1152.11	0.22	1173.78	0.15	1207.61	0.10		
1.9	1152.52	0.15	1175.58	0.10	1209.49	0.07		
2.12	1152.96	0.15	1177.05	0.09	1210.63	0.07		
2.53	1153.65	0.15	1179.44	0.10	1213.20	0.08		
2.7	1153.76	0.12	1180.18	0.11	1213.69	0.06		
3.03	1154.52	0.12	1182.26	0.11	1215.58	0.07		
3.23	1154.72	0.12	1183.26	0.10	1216.69	0.06		
3.64	1155.74	0.10	1185.31	0.08	1218.81	0.06		
3.89	1156.07	0.11	1186.67	0.10	1219.98	0.06		
4.25	1156.87	0.11	1188.70	0.10	1221.91	0.06		
4.62	1157.63	0.11	1190.66	0.09	1223.78	0.06		
4.92	1158.12	0.12	1191.97	0.10	1224.97	0.08		
5.12	1158.50	0.11	1193.07	0.09	1226.13	0.06		
5.45	1159.36	0.14	1194.65	0.11	1227.70	0.08		
6.07	1160.36	0.12	1197.44	0.11	1230.20	0.07		
6.29	1161.06	0.12	1198.48	0.11	1231.29	0.07		
6.57	1162.08	0.08	1200.03	0.08	1232.77	0.05		
6.74	1162.57	0.10	1200.99	0.09	1233.71	0.06		
7.05	1163.21	0.08	1202.63	0.07	1235.15	0.05		
7.33	1163.84	0.09	1203.86	0.07	1236.36	0.05		
7.53	1164.37	0.09	1204.82	0.08	1237.23	0.05		
7.87	1164.86	0.11	1206.13	0.10	1238.52	0.06		
8.29	1165.87	0.09	1208.24	0.07	1240.52	0.05		
8.49	1166.42	0.24	1210.76	0.22	1244.77	0.10		
8.06	1165.41	0.65			1244.08	0.23		

	c1-decompression series							
p	v107	SE	v119	SE	v192*	SE	v188	SE
7.98					192.34	0.08		
7.75					192.01	0.08		
7.56					191.74	0.07		
7.28					191.15	0.09		
7.05					190.74	0.09		
6.8					190.33	0.10		
6.55					189.67	0.08		
6.21					189.06	0.10		
6.04					188.67	0.10		
5.78					188.21	0.09		
5.48					187.67	0.10		
5.29					187.26	0.10		
4.98					186.78	0.10		
4.7					186.46	0.12		
4.39					185.78	0.12		
3.53	109.93	0.21			184.54	0.11	202.79	0.08
3.25	108.79	0.22			184.00	0.13	201.53	0.10
2.34	108.84	0.16	134.47	0.29	180.79	0.14	197.74	0.04
1.98	108.17	0.17	130.94	0.29	178.93	0.36	196.10	0.06
1.48	108.10	0.08	127.64	0.26	175.68	0.15	194.53	0.02
1.15	107.81	0.06	125.01	0.12	174.11	0.16	193.32	0.02

	c1-decompression series							
p	v230*	SE	v288*	SE	v457*	SE	v458	SE
7.98	230.75	0.04	288.27	0.16	457.47	0.06		
7.75	230.06	0.04	287.86	0.17	457.54	0.07		
7.56	229.81	0.04	286.28	0.18	457.22	0.07		
7.28	229.15	0.04	285.10	0.17	456.93	0.08		
7.05	228.61	0.04	284.01	0.17	456.75	0.07		
6.8	228.25	0.05	282.66	0.19	456.39	0.07		
6.55	227.44	0.04	281.38	0.14	456.14	0.06		
6.21	226.62	0.05	280.12	0.19	455.78	0.08		
6.04	226.10	0.05	279.19	0.20	455.54	0.08		
5.78	225.45	0.05	278.20	0.23	455.26	0.08		
5.48	224.71	0.04	276.80	0.17	454.95	0.06		
5.29	224.23	0.04	275.86	0.20	454.61	0.07		
4.98	223.48	0.04	274.62	0.20	454.43	0.07		
4.7	223.09	0.04	273.65	0.25	454.08	0.08		
4.39	222.33	0.04	272.03	0.26	453.51	0.09		
3.53	219.57	0.04	268.79	0.29	452.40	0.12	461.34	0.14
3.25	218.64	0.06	267.73	0.40	451.79	0.14	460.58	0.16
2.34	216.34	0.05	265.00	0.48	450.77	0.28	460.24	0.10
1.98	215.38	0.32	261.55	3.35	449.59	0.50	459.77	0.09
1.48	206.19	1.95					459.57	0.03
1.15	211.89	0.66					459.41	0.03

	c1-decompression series							
p	v499*	SE	v497	SE	v604	SE	v617*	SE
7.98	499.74	0.12					617.99	0.01
7.75	499.74	0.09					617.89	0.01
7.56	499.05	0.11					617.67	0.01
7.28	498.68	0.11					617.30	0.01
7.05	498.22	0.10					617.02	0.01
6.8	497.79	0.12					616.68	0.01
6.55	497.14	0.10					616.34	0.01
6.21	496.64	0.13					615.91	0.01
6.04	496.45	0.15					615.64	0.01
5.78	496.05	0.14					615.38	0.01
5.48	495.63	0.11					614.95	0.01
5.29	495.31	0.13					614.66	0.01
4.98	494.99	0.12					614.44	0.01
4.7	494.64	0.16					614.12	0.02
4.39	494.05	0.15					613.55	0.02
3.53	493.75	0.12	514.83	0.28	607.58	0.03	612.53	0.03
3.25	493.31	0.16	513.59	0.38	607.35	0.04	612.33	0.03
2.34	491.39	0.13	509.26	0.22	606.48	0.02	611.35	0.04
1.98	490.21	0.40	507.35	0.21	606.33	0.02		
1.48	488.55	0.28	505.18	0.11	605.80	0.01		
1.15	487.14	0.37	503.77	0.10	605.48	0.01		

	c1-decompression series							
p	v706*	SE	v931	SE	v1051*	SE	v1057	SE
7.98	706.21	0.30			1051.88	0.01		
7.75	705.85	0.28			1051.38	0.01		
7.56	705.23	0.25			1049.97	0.01		
7.28	704.67	0.31			1049.12	0.01		
7.05	704.22	0.30			1048.33	0.01		
6.8	703.58	0.33			1047.14	0.01		
6.55	702.81	0.29			1045.95	0.01		
6.21	702.52	0.36			1044.91	0.01		
6.04	702.00	0.35			1044.20	0.01		
5.78	701.11	0.33			1043.31	0.01		
5.48	700.89	0.36			1042.36	0.01		
5.29	700.52	0.30			1041.64	0.01		
4.98	699.77	0.35			1040.68	0.01		
4.7	699.45	0.40			1039.91	0.01		
4.39	698.77	0.42			1038.53	0.01		
3.53			948.07	0.11	1035.66	0.01	1070.53	0.03
3.25			947.14	0.12	1034.81	0.01	1069.65	0.05
2.34			942.79	0.05	1031.95	0.01	1065.98	0.02
1.98			940.80	0.06	1030.37	0.06	1064.33	0.03
1.48			938.73	0.03	1029.09	0.15	1062.71	0.02
1.15			937.44	0.03	1028.27	0.14	1061.83	0.01

	c1-decompression series							
p	v1113*	SE	v1150	SE	v1162	SE	v1197	SE
7.98	1113.49	0.08						
7.75	1113.52	0.07						
7.56	1113.06	0.08						
7.28	1112.76	0.08						
7.05	1112.53	0.08						
6.8	1112.05	0.09						
6.55	1111.73	0.07						
6.21	1111.56	0.09						
6.04	1111.37	0.09						
5.78	1111.10	0.09						
5.48	1110.84	0.06						
5.29	1110.60	0.07						
4.98	1110.35	0.06						
4.7	1110.15	0.07						
4.39	1109.63	0.06						
3.53	1108.25	0.05	1154.84	0.37	1186.70	0.35	1219.60	0.14
3.25	1107.77	0.07	1154.38	0.51	1184.32	0.37	1218.33	0.19
2.34	1105.93	0.07	1152.90	0.31	1179.40	0.39	1212.51	0.10
1.98	1105.04	0.22	1152.78	0.30	1176.11	0.16	1209.66	0.14
1.48			1151.91	0.18	1173.70	0.11	1207.15	0.06
1.15	1103.74	0.37	1151.97	0.23	1171.91	0.09	1205.63	0.06

	c1-decompression series						
p	v1244*	SE					
7.98	1244.75	0.10					
7.75	1244.49	0.10					
7.56	1243.34	0.08					
7.28	1242.77	0.10					
7.05	1242.00	0.09					
6.8	1241.12	0.10					
6.55	1240.13	0.08					
6.21	1239.64	0.10					
6.04	1239.08	0.09					
5.78	1238.42	0.08					
5.48	1237.63	0.09					
5.29	1237.22	0.07					
4.98	1236.33	0.07					
4.7	1235.86	0.09					
4.39	1234.85	0.08					
3.53	1232.86	0.11					
3.25	1232.07	0.15					
2.34	1229.26	0.16					
1.98	1226.66	0.43					
1.48							
1.15							

	c2-compression series							
p	v106	SE	v114	SE	v136	SE	v165	SE
1Atm	106.97	0.05	114.02	0.06			165.83	0.10
0.47	108.20	0.04	118.92	0.06			169.85	0.09
0.74	108.47	0.03	121.20	0.04	136.29	0.66	171.58	0.08
1.07	108.76	0.03	124.05	0.05	137.96	0.62	173.65	0.07
1.35	108.93	0.04	126.09	0.03	139.36	0.27	175.01	0.07
1.57	109.12	0.07	127.83	0.04	140.57	0.26	176.29	0.11
1.9	109.45	0.05	130.14	0.04	142.14	0.36	177.74	0.12
2.12	109.74	0.03	132.03	0.03	143.37	0.26	178.92	0.10
2.53	110.15	0.05	135.08	0.04	145.45	0.40	180.71	0.17
2.7	110.28	0.04	135.74	0.03	145.94	0.27	181.12	0.13
3.03	110.61	0.08	138.44	0.06	147.88	0.64	182.69	0.28
3.23	110.85	0.03	139.65	0.03	148.54	0.28	183.37	0.11
3.64	111.22	0.03	142.50	0.03	150.54	0.28	184.82	0.12
3.89	111.49	0.03	144.20	0.04	151.67	0.36	185.68	0.12
4.25	111.95	0.04	146.62	0.05	153.27	0.34	187.02	0.17
4.62	112.42	0.03	149.00	0.05	155.14	0.35	188.11	0.15
4.92	112.52	0.03	150.48	0.06	155.98	0.44	188.93	0.11
5.12	112.89	0.03	152.17	0.04			189.63	0.13
5.45	113.05	0.04	153.50	0.09	158.53	0.56	190.44	0.16
6.07	113.90	0.05	157.24	0.06			192.12	0.19
6.29	114.06	0.04	158.40	0.05			192.74	0.17
6.57	114.35	0.07	160.04	0.14	187.22	0.67	193.19	0.24
6.74	114.72	0.13	161.79	0.35	188.15	0.59	193.81	0.26
7.05	114.84	0.08	163.84	0.24	189.99	0.14		
7.33	114.16	0.40	165.34	1.24	190.53	0.17		
7.53	118.96	1.02			191.49	0.10		
7.87					192.34	0.17		
8.29					193.22	0.13		
8.49					193.73	0.10		
8.06					192.83	0.14		

	c2-compression series							
p	v188	SE	v201	SE	v202	SE	v270	SE
1Atm	188.16	0.02			202.12	0.33	270.04	0.57
0.47	190.68	0.02			207.36	0.39	271.70	0.51
0.74	191.72	0.02	201.32	0.26	211.52	0.40	272.21	0.42
1.07	193.02	0.02	203.24	0.22	214.48	0.38	273.36	0.43
1.35	193.81	0.03	204.74	0.20	216.64	0.52	272.93	0.35
1.57	194.54	0.05	206.04	0.28	218.43	0.98	272.89	0.39
1.9	195.78	0.03	208.01	0.36	221.16	0.53	275.25	0.43
2.12	196.70	0.03	209.39	0.25	222.83	0.44	275.90	0.32
2.53	198.20	0.04	212.00	0.41	225.97	0.73	277.34	0.55
2.7	198.52	0.03	212.58	0.29	226.93	0.52	277.47	0.36
3.03	199.91	0.05	214.86	0.55	229.54	1.06	278.81	0.74
3.23	200.53	0.02	216.10	0.26	230.63	0.49	277.05	22.13
3.64	201.98	0.02	218.74	0.27	233.44	0.54	278.20	20.78
3.89	202.87	0.02	220.37	0.28	235.11	0.53		
4.25	204.17	0.03	222.91	0.39	237.58	1.03	278.36	2.57
4.62	205.46	0.02	225.61	0.40	240.17	0.74	280.99	5.02
4.92	206.15	0.02	227.28	0.33	241.66	0.80	280.52	0.96
5.12	206.99	0.02	228.80	0.34	243.21	0.95	282.16	2.21
5.45	207.81	0.02	230.51	0.38	245.21	1.32	282.49	0.95
6.07	209.70	0.03	233.81	0.40	248.41	1.37	283.96	1.23
6.29	210.31	0.02	234.84	0.35	250.48	1.02	285.05	1.56
6.57	211.43	0.03	236.48	0.77	251.73	2.23	283.00	2.48
6.74	212.76	0.06	238.53	1.09			283.56	0.98
7.05	214.03	0.06	227.42	0.08			284.22	0.27
7.33	215.94	0.32	230.11	0.04			284.62	0.26
7.53	226.55	2.84	231.01	0.08			286.12	0.13
7.87			232.09	0.06			286.97	0.25
8.29			233.76	0.03			288.38	0.16
8.49			234.35	0.02			289.40	0.14
8.06			233.03	0.03			287.51	0.23

	c2-compression series							
p	v352	SE	v458	SE	v481	SE	v497	SE
1Atm			458.74	0.04	481.89	0.41	497.96	0.08
0.47	352.29	2.03	459.14	0.04	484.30	0.38	500.79	0.08
0.74	352.89	2.02	459.06	0.04	485.39	0.34	501.96	0.07
1.07	353.86	1.73	459.15	0.04	486.82	0.29	503.62	0.07
1.35	354.53	1.52	459.18	0.05	487.90	0.19	504.72	0.08
1.57	355.74	1.95	459.35	0.07	488.90	0.23	505.70	0.14
1.9	355.22	3.00	459.33	0.06	490.03	0.30	506.93	0.09
2.12	356.91	1.96	459.55	0.05	490.68	0.23	508.13	0.07
2.53	357.43	2.88	459.90	0.07	492.51	0.40	510.00	0.11
2.7	358.08	1.99	459.93	0.05	492.39	0.24	510.33	0.08
3.03	358.75	4.54	460.25	0.10	494.09	0.52	511.92	0.17
3.23	359.06	1.73	460.31	0.04	494.52	0.25	512.73	0.07
3.64	360.35	1.79	460.64	0.04	496.23	0.27	514.53	0.06
3.89			460.90	0.03	497.57	0.32	515.70	0.06
4.25	361.74	2.37	461.23	0.06	499.58	0.50	517.30	0.10
4.62	362.39	1.91	461.46	0.04	501.32	0.52	518.78	0.07
4.92	362.69	1.50	461.64	0.04	502.01	0.41	519.75	0.07
5.12	363.09	1.48	461.88	0.05	503.24	0.53	520.79	0.09
5.45	363.62	1.92	462.14	0.05	505.86	81.97	521.76	0.26
6.07	365.02	1.98	462.36	0.06	507.11	0.69	523.93	0.13
6.29	365.79	1.43	462.34	0.04	507.64	0.52	524.65	0.10
6.57	367.11	2.21	462.12	0.05	507.60	0.66	525.85	0.11
6.74	370.42	3.40	461.52	0.10	510.01	1.36	526.44	0.32
7.05	368.75	2.86	463.39	0.34			528.03	0.09
7.33	387.78	1.53	456.94	0.11	498.33	0.12	528.95	0.53
7.53	390.19	0.90	456.44	0.06	498.70	0.09	529.14	0.99
7.87	391.62	1.38	456.36	0.10	498.69	0.12		
8.29	393.47	1.11	456.50	0.08	499.13	0.08		
8.49			456.63	0.05	499.37	0.06		
8.06	392.80	1.45	456.58	0.10	498.93	0.09		

	c2-compression series							
p	v578	SE	v604	SE	v931	SE	v1057	SE
1Atm	578.14	0.33	604.89	0.01	931.31	0.03	1057.11	0.02
0.47	579.49	0.32	605.39	0.01	934.12	0.03	1059.25	0.02
0.74	579.99	0.22	605.35	0.01	935.49	0.04	1060.33	0.02
1.07	580.91	0.31	605.61	0.01	937.21	0.03	1061.59	0.01
1.35	581.43	0.19	605.67	0.02	938.48	0.04	1062.53	0.01
1.57	582.02	0.27	605.76	0.04	939.49	0.07	1063.31	0.02
1.9	582.57	0.28	605.87	0.02	940.82	0.11	1064.35	0.01
2.12	583.30	0.21	606.15	0.02	941.91	0.09	1065.29	0.01
2.53	584.33	0.40	606.38	0.03	943.81	0.15	1066.66	0.02
2.7	584.36	0.26	606.40	0.02	944.34	0.11	1066.96	0.01
3.03	585.49	0.54	606.68	0.04			1068.26	0.02
3.23	585.66	0.30	606.78	0.02	946.90	0.09	1068.84	0.01
3.64	586.51	0.39	607.12	0.01	948.68	0.09	1070.26	0.01
3.89	587.23	0.49	607.38	0.01	949.76	0.07	1071.04	0.01
4.25	587.87	0.73	607.66	0.02	951.25	0.13	1072.23	0.01
4.62	590.62	0.23	607.97	0.01	952.85	0.08	1073.38	0.01
4.92	590.97	0.17	608.11	0.01	954.08	0.07	1074.21	0.01
5.12	591.39	0.20	608.34	0.01	954.99	0.09	1074.94	0.01
5.45	591.76	0.21	608.65	0.02	956.01	0.11	1075.74	0.01
6.07	592.30	0.26	609.05	0.02	958.57	0.11	1077.59	0.01
6.29	592.56	0.22	609.15	0.01	959.61	0.07	1078.24	0.01
6.57	592.91	0.48	609.59	0.01	960.18	0.07	1079.12	0.01
6.74	593.34	0.56	610.41	0.03	960.17	0.13	1079.64	0.03
7.05	594.03	0.71	610.15	0.02	961.48	0.11	1080.86	0.02
7.33			615.96	0.02	960.24	0.78	1081.62	0.09
7.53			616.47	0.01			1081.89	0.22
7.87			616.99	0.02				
8.29			617.36	0.02			1052.17	0.01
8.49			617.45	0.01			1052.79	0.01
8.06			617.33	0.02			1051.27	0.01

	c2-compression series							
p	v1150	SE	v1163	SE	v1197	SE		
1Atm	1150.23	0.12	1163.42	0.07	1197.44	0.05		
0.47	1150.91	0.11	1167.22	0.08	1201.12	0.05		
0.74	1151.13	0.10	1169.08	0.08	1202.83	0.04		
1.07	1151.69	0.12	1171.06	0.07	1204.95	0.04		
1.35	1151.89	0.12	1174.20	0.15	1206.47	0.04		
1.57	1152.21	0.20	1176.24	0.15	1207.80	0.05		
1.9	1152.38	0.23	1176.58	0.10	1209.63	0.07		
2.12	1152.85	0.16	1178.02	0.08	1210.86	0.05		
2.53	1153.49	0.28	1179.95	0.10	1213.25	0.10		
2.7	1153.53	0.17	1180.47	0.07	1213.86	0.06		
3.03	1154.04	0.31	1182.45	0.14	1215.90	0.13		
3.23	1154.44	0.16	1183.32	0.06	1216.83	0.06		
3.64	1155.15	0.17	1185.54	0.05	1219.00	0.06		
3.89	1155.62	0.17	1186.80	0.05	1220.27	0.06		
4.25	1156.37	0.24	1188.67	0.08	1222.10	0.08		
4.62	1157.00	0.19	1190.66	0.06	1223.94	0.07		
4.92	1157.57	0.15	1191.96	0.05	1225.13	0.06		
5.12	1158.04	0.19	1193.16	0.07	1226.36	0.07		
5.45	1158.57	0.25	1194.49	0.08	1227.54	0.08		
6.07	1159.95	0.22	1197.42	0.08	1230.38	0.09		
6.29	1160.54	0.19	1198.43	0.06	1231.40	0.08		
6.57	1161.11	0.23	1200.02	0.10	1232.84	0.11		
6.74	1161.22	0.40	1200.99	0.21	1233.59	0.20		
7.05	1161.79	0.31	1203.08	0.13	1236.11	0.53		
7.33			1204.25	0.64				
7.53								
7.87								
8.29	1113.07	0.07						
8.49	1113.22	0.06						
8.06	1112.94	0.11						

	c1-decompression series							
p	v106	SE	v114	SE	v192*	SE	v188	SE
7.98					192.83	0.12		
7.75					192.53	0.10		
7.56					192.19	0.11		
7.28					191.57	0.13		
7.05					191.14	0.12		
6.8					190.51	0.17		
6.55					189.99	0.11		
6.21					189.33	0.18		
6.04					188.83	0.38		
5.78					188.53	0.08		
5.48					187.87	0.15		
5.29					187.64	0.08		
4.98					187.09	0.06		
4.7					186.62	0.06		
3.78					185.93	0.06		
4.39					184.97	0.10		
3.53					184.48	0.11		
3.25					183.88	0.11		
2.34					182.26	1.06		
1.98	108.21	0.17	130.38	0.25	178.52	0.32	195.89	0.09
1.48	108.15	0.13	126.96	0.17	175.55	0.20	194.32	0.06
1.15	107.86	0.05	124.75	0.09	173.89	0.06	193.30	0.03

	c1-decompression series							
p	v232*	SE	v287*	SE	v392*	SE	v456*	SE
7.98	232.71	0.02	287.42	0.19	392.06	1.21	456.86	0.09
7.75	231.99	0.02	286.75	0.13	392.04	0.86	456.89	0.07
7.56	231.45	0.03	286.09	0.15	391.06	0.98	456.87	0.07
7.28	230.32	0.03	284.84	0.18	389.99	1.24	456.58	0.08
7.05	229.85	0.03	284.07	0.16	388.95	1.09	456.52	0.07
6.8	229.12	0.04	282.86	0.21	387.17	2.04	456.23	0.10
6.55	228.41	0.03	281.56	0.17	386.66	1.01	455.96	0.08
6.21	227.28	0.04	280.21	0.25	384.52	1.33	455.64	0.10
6.04	226.73	0.09	279.65	0.49	384.60	3.02	455.52	0.21
5.78	226.08	0.02	278.53	0.12	383.19	0.70	455.26	0.04
5.48	225.02	0.04	277.44	0.20	382.62	1.54	454.80	0.07
5.29	224.89	0.02	276.40	0.12	381.07	0.61	454.55	0.04
4.98	224.01	0.02	275.14	0.10	380.56	0.54	454.30	0.03
4.7	223.63	0.02	274.08	0.09	379.08	0.52	453.95	0.03
3.78	222.59	0.03	272.22	0.08	376.84	0.43	453.41	0.03
4.39	221.07	0.02	269.89	0.16	374.75	0.80	452.78	0.05
3.53	220.33	0.03	268.84	0.18	373.94	0.76	452.64	0.05
3.25	219.47	0.03	267.55	0.20	371.48	0.97	452.09	0.06
2.34	216.90	0.15	263.63	1.77	366.46	9.79	451.00	0.53
1.98	215.54	0.10					458.70	0.15
1.48	212.10	0.99					459.56	0.09
1.15							459.34	0.03

	c1-decompression series							
p	v498*	SE	v497	SE	v617*	SE	v706*	SE
7.98	498.93	0.08			617.77	0.02	706.39	0.40
7.75	498.80	0.07			617.80	0.01	705.81	0.32
7.56	498.63	0.07			617.66	0.01	705.27	0.34
7.28	498.08	0.09			617.25	0.02	704.73	0.36
7.05	497.88	0.08			617.15	0.01	704.07	0.37
6.8	497.49	0.11			616.78	0.02	703.66	0.49
6.55	496.89	0.08			616.51	0.01	703.09	0.36
6.21	496.45	0.11			616.05	0.02	702.46	0.54
6.04	496.43	0.28			615.86	0.05	701.65	1.32
5.78	496.06	0.06			615.54	0.01	701.31	0.25
5.48	495.69	0.13			615.06	0.02	701.02	0.45
5.29	495.33	0.06			614.79	0.01	700.50	0.23
4.98	494.91	0.05			614.47	0.01	700.27	0.19
4.7	494.61	0.05			614.06	0.01	699.81	0.18
3.78	494.08	0.06			613.53	0.01	698.95	0.15
4.39	493.32	0.07			612.88	0.01		
3.53	493.09	0.10			612.66	0.01	697.28	0.29
3.25	492.61	0.11			612.23	0.01	696.72	0.35
2.34	491.40	0.73			611.25	0.15	684.61	18.54
1.98	490.13	0.29	506.98	0.22	607.71	0.05		
1.48	487.94	0.46	505.18	0.22	605.91	0.03		
1.15	486.98	0.14	503.68	0.08	605.47	0.01		

	c1-decompression series							
p	v931	SE	v1051*	SE	v1057	SE	v1113*	SE
7.98			1051.10	0.01			1113.35	0.09
7.75			1050.60	0.01			1113.22	0.07
7.56			1049.92	0.01			1113.02	0.07
7.28			1048.76	0.01			1112.82	0.08
7.05			1048.12	0.01			1112.66	0.08
6.8			1047.19	0.01			1112.31	0.10
6.55			1046.10	0.01			1111.99	0.07
6.21			1045.05	0.01			1111.77	0.10
6.04			1044.44	0.03			1111.68	0.21
5.78			1043.60	0.01			1111.28	0.04
5.48			1042.58	0.01			1111.01	0.07
5.29			1041.91	0.01			1110.68	0.04
4.98			1040.82	0.00			1110.39	0.03
4.7			1040.06	0.00			1109.97	0.02
3.78			1038.68	0.00			1109.36	0.02
4.39			1036.89	0.01			1108.57	0.03
3.53			1036.13	0.01			1108.25	0.03
3.25			1035.00	0.01			1107.67	0.03
2.34			1031.94	0.05			1105.83	0.35
1.98	938.80	0.96	1030.03	0.16	1064.18	0.20	1103.87	0.93
1.48	937.97	0.18	1028.63	0.25	1062.60	0.08		
1.15	936.90	0.05	1027.67	0.31	1061.70	0.03	1099.20	0.41

	c1-decompression series							
p	v1197	SE	v1244*	SE				
7.98			1244.36	0.16				
7.75			1243.91	0.12				
7.56			1243.45	0.13				
7.28			1242.61	0.13				
7.05			1241.96	0.12				
6.8			1241.27	0.19				
6.55			1240.55	0.11				
6.21			1239.55	0.17				
6.04			1239.47	0.38				
5.78			1238.85	0.07				
5.48			1238.10	0.12				
5.29			1237.63	0.06				
4.98			1236.79	0.05				
4.7			1236.18	0.04				
3.78			1235.16	0.04				
4.39			1233.78	0.06				
3.53			1233.16	0.06				
3.25			1232.06	0.07				
2.34			1229.30	0.80				
1.98	1209.41	0.45						
1.48	1207.26	0.18						
1.15	1205.54	0.04						

	c3-compression series							
p	v107	SE	v113	SE	v165	SE	v187	SE
1Atm	107.12	1.26	113.21	0.66	165.46	0.27	187.55	0.17
0.47	107.71	0.40	118.75	0.32	169.77	0.08	190.32	0.04
0.74	107.75	0.24	121.00	0.12	171.48	0.07	191.29	0.04
1.07	108.08	0.09	123.94	0.06	173.54	0.03	192.64	0.02
1.35	108.56	0.05	126.06	0.02	175.09	0.27	193.81	0.05
1.57	108.65	0.07	127.72	0.02	176.19	1.08	194.66	0.06
1.9	108.95	0.09	130.12	0.03	177.31	1.39	195.79	0.08
2.12	109.39	0.06	131.96	0.02	178.85	0.70	196.66	0.06
2.53	109.96	0.05	135.05	0.02	180.72	0.83	198.22	0.04
2.7	110.10	0.05	135.79	0.02			198.59	0.04
3.03	110.76	0.05	138.46	0.02	182.62	0.77	199.99	0.04
3.23	110.99	0.05	139.73	0.02			200.64	0.04
3.64	111.59	0.05	142.62	0.02	185.27	13.43	202.15	0.04
3.89	111.77	0.05	144.22	0.02	185.71	0.70	202.98	0.04
4.25	112.49	0.05	146.76	0.02	187.13	0.84	204.32	0.04
4.62	113.28	0.05	149.22	0.02			205.65	0.04
4.92	113.41	0.05	150.84	0.02			206.49	0.04
5.12	113.93	0.06	152.38	0.02			207.40	0.04
5.45	114.34	0.06	154.13	0.02	190.41	0.91	208.32	0.04
6.07	115.17	0.05	157.56	0.02	191.95	1.17	210.27	0.03
6.29	116.58	0.05	159.05	0.02	192.68	0.45	211.09	0.04
6.57	116.85	0.06	160.57	0.02	193.63	2.43	212.00	0.04
6.74	117.41	0.06	161.90	0.02	194.23	0.55	212.83	0.04
7.05	117.99	0.07	163.84	0.02	195.07	0.60	213.96	0.04
7.33	118.04	0.06	165.16	0.02	195.47	0.32	214.70	0.04
7.53	118.31	0.06	166.26	0.02	196.05	0.56	215.42	0.04
7.87	118.60	0.08	168.19	0.02	196.73	0.50	216.72	0.06
8.29	116.96	0.21	170.40	0.06			218.08	0.13
8.49	113.84	0.77	173.19	0.11				
8.06	111.32	0.97	169.62	0.13				

	c3-compression series							
p	v200	SE	v211	SE	v211a	SE	v211b	SE
1Atm								
0.47	200.06	0.31						
0.74	201.36	0.27	211.53	3.05				
1.07	203.06	0.12	213.60	1.37				
1.35			216.79	0.45				
1.57			218.57	0.55				
1.9			220.75	0.72				
2.12	209.55	1.71	222.98	0.59				
2.53			226.11	0.46				
2.7			226.86	0.52				
3.03	215.23	1.49	229.54	0.55				
3.23			230.93	0.60				
3.64			233.27	0.68				
3.89			234.42	0.90				
4.25			236.13	1.19				
4.62			237.44	1.70				
4.92					242.58	1.36	229.58	1.15
5.12					244.30	1.40	230.85	0.97
5.45					245.43	1.40	231.43	0.62
6.07					250.07	1.30	233.35	0.48
6.29					250.69	1.68	234.47	0.51
6.57					252.26	2.63	234.65	0.56
6.74					254.01	1.75	234.64	0.48
7.05					255.93	2.07	235.36	0.55
7.33					257.15	0.82	235.31	0.49
7.53					258.24	3.04	235.62	0.63
7.87							231.21	0.46
8.29							230.45	0.16
8.49							232.24	0.02
8.06							231.25	0.03

	c3-compression series							
p	v226	SE	v267	SE	v267a	SE	v267b	SE
1Atm	226.16	1.79	267.69	1.48				
0.47	227.07	0.43	269.12	0.49				
0.74	227.30	0.57	269.74	0.33				
1.07	227.33	0.39	270.79	0.17				
1.35			273.81	0.46				
1.57			275.31	0.87				
1.9			276.56	1.02				
2.12			277.49	0.67				
2.53			278.76	0.58				
2.7			279.07	0.61				
3.03			280.41	0.54				
3.23			281.27	0.68				
3.64			282.79	0.58				
3.89			283.01	0.57				
4.25			284.60	0.58				
4.62					288.60	5.37	281.50	7.67
4.92					288.17	2.13	280.06	2.42
5.12					290.13	2.11	281.83	2.34
5.45					290.76	1.44	282.30	1.15
6.07					293.88	0.81	284.46	0.99
6.29					295.13	0.99	284.97	1.04
6.57					296.19	0.82	286.21	1.04
6.74					297.29	0.81	286.48	1.00
7.05					298.92	0.73	287.71	0.78
7.33					300.05	0.63	288.34	0.67
7.53					301.18	0.63	289.43	1.06
7.87					302.52	0.72	289.75	0.55
8.29					304.92	1.61	290.55	0.54
8.49							291.33	0.24
8.06							289.42	0.30

	c3-compression series							
p	v459	SE	v482	SE	v498	SE	v585	SE
1Atm	459.01	0.15	482.51	1.23	498.23	38.20	585.47	0.69
0.47	459.52	0.03	482.99	0.32	502.09	0.67	580.14	0.73
0.74	459.49	0.03	484.37	0.27	503.21	0.40	580.46	0.49
1.07	459.63	0.02	486.26	0.10	503.89	0.14	581.32	0.28
1.35	459.49	0.10	493.47	2.59	504.87	0.10	581.34	0.14
1.57	459.62	0.15			505.17	0.11	581.67	0.13
1.9	459.69	0.18			506.52	0.14	582.53	0.16
2.12	459.91	0.12	498.56	4.00	508.11	0.11	583.25	0.12
2.53	460.14	0.09	495.74	8.59	509.93	0.08	584.13	0.10
2.7	460.30	0.10			510.11	0.08	584.34	0.10
3.03	460.47	0.09	502.39	3.47	512.05	0.09	585.19	0.11
3.23	460.53	0.09			512.47	0.08	585.54	0.12
3.64	461.08	0.09	504.29	4.77	514.86	0.10	586.74	0.11
3.89	461.21	0.10	504.81	4.61	515.79	0.10	587.46	0.11
4.25	461.45	0.09	505.83	5.55	517.32	0.09	588.17	0.11
4.62	461.84	0.10	504.75	5.79	518.92	0.11	588.91	0.12
4.92	462.05	0.09	506.29	6.82	520.05	0.09	589.66	0.09
5.12	462.37	0.10			520.73	0.09	590.28	0.11
5.45	462.49	0.10	507.46	7.08	522.12	0.09	590.82	0.09
6.07	462.78	0.10	509.58	6.16	524.39	0.08	591.87	0.09
6.29	462.94	0.10	509.67	1.00	525.35	0.12	592.24	0.08
6.57	462.94	0.11	506.22	3.01	526.30	0.08	592.62	0.08
6.74	463.14	0.11	512.10	1.09	527.41	0.12	593.11	0.07
7.05	463.22	0.11			528.72	0.07	593.65	0.08
7.33	463.07	0.10	513.99	0.79	529.75	0.09	593.85	0.07
7.53	463.16	0.10	512.50	10.24	530.78	0.06	594.26	0.08
7.87	462.97	0.12	516.40	0.90	531.86	0.11	594.65	0.07
8.29	461.23	0.23	519.24	2.22	533.73	0.23	595.82	0.23
8.49	459.65	0.23	500.31	0.17	535.22	1.22	596.95	0.51
8.06	459.05	0.19	499.77	0.16	532.08	0.53	595.82	0.45

	c3-compression series							
p	v604	SE	v931	SE	v1056	SE	v1151	SE
1Atm	604.79	0.34	931.47	0.05	1056.23	0.14		
0.47	605.20	0.14	934.26	0.01	1059.30	0.02		
0.74	605.20	0.11	935.65	0.01	1060.35	0.02	1151.61	0.42
1.07	605.53	0.03	937.36	0.01	1061.60	0.01	1152.32	0.23
1.35	605.64	0.04	938.70	0.16	1062.69	0.01	1151.92	0.18
1.57	605.63	0.07	939.93	0.29	1063.44	0.01	1152.10	0.09
1.9	605.80	0.09			1064.56	0.02	1152.47	0.12
2.12	606.03	0.06	942.29	0.28	1065.39	0.01	1152.94	0.09
2.53	606.30	0.05	944.84	0.23	1066.80	0.01	1153.56	0.08
2.7	606.34	0.05	945.35	0.25	1067.14	0.01	1153.75	0.08
3.03	606.57	0.04	946.98	0.22	1068.43	0.01	1154.51	0.08
3.23	606.66	0.05	948.04	0.28	1069.11	0.01	1154.89	0.09
3.64	607.19	0.04	949.67	0.22	1070.46	0.01	1155.63	0.08
3.89	607.33	0.06	950.63	0.21	1071.19	0.01	1155.90	0.07
4.25	607.52	0.05	952.51	0.21	1072.48	0.01	1156.83	0.07
4.62	607.87	0.05	954.38	0.26	1073.73	0.01	1157.78	0.08
4.92	608.16	0.05	955.18	0.20	1074.48	0.01	1158.11	0.07
5.12	608.41	0.06	956.37	0.26	1075.29	0.01	1158.76	0.08
5.45	608.58	0.06	957.63	0.22	1076.22	0.01	1159.40	0.07
6.07	609.06	0.05	959.98	0.21	1077.98	0.01	1160.73	0.08
6.29	609.10	0.05	962.11	0.19	1078.80	0.01	1161.87	0.08
6.57	609.27	0.06	963.12	0.24	1079.68	0.01	1162.45	0.09
6.74	609.52	0.06	964.28	0.25	1080.33	0.01	1162.94	0.08
7.05	609.68	0.07	965.98	0.28	1081.42	0.01	1163.90	0.09
7.33	609.64	0.05	967.12	0.18	1082.21	0.01	1164.65	0.09
7.53	609.89	0.06	968.29	0.28	1082.82	0.01	1165.09	0.10
7.87	610.33	0.11	968.59	0.21	1083.73	0.01	1165.47	0.09
8.29	609.38	1.76	968.25	0.71	1085.09	0.02	1165.75	0.20
8.49	605.41	0.10			1086.68	0.03		
8.06	617.64	0.04			1084.59	0.03	1164.38	0.52

	c3-compression series							
p	v1157	SE	v1175	SE	v1196	SE		
1Atm	1157.81	1.29	1175.33	0.78	1196.96	0.22		
0.47	1161.55	0.19	1176.11	0.17	1200.84	0.05		
0.74	1162.54	0.15	1175.89	0.32	1202.58	0.04		
1.07	1163.65	0.07	1175.95	0.19	1204.70	0.02		
1.35	1163.62	0.48	1173.11	0.35	1206.26	0.14		
1.57			1173.66	0.12	1207.66	0.86		
1.9			1175.49	0.15	1209.65	0.74		
2.12			1176.93	0.10	1210.99	0.41		
2.53	1168.87	0.36	1179.69	0.11	1213.33	0.38		
2.7	1169.19	0.38	1180.28	0.11	1213.89	0.46		
3.03			1181.94	0.09	1215.90	0.36		
3.23	1171.32	0.33	1183.45	0.10	1216.64	0.45		
3.64	1172.50	0.22	1185.68	0.09	1218.66	0.38		
3.89	1173.06	0.15	1186.88	0.09	1219.90	0.33		
4.25	1174.29	0.16	1188.92	0.09	1222.01	0.35		
4.62	1175.48	0.19	1190.95	0.10	1223.72	0.43		
4.92	1176.01	0.12	1192.25	0.09	1225.16	0.30		
5.12	1176.75	0.14	1193.49	0.10	1226.28	0.38		
5.45	1177.66	0.12	1195.01	0.09	1227.80	0.30		
6.07	1179.14	0.13	1197.92	0.09	1230.57	0.26		
6.29	1180.22	0.11	1199.18	0.08	1231.81	0.23		
6.57	1180.98	0.12	1200.59	0.09	1233.18	0.27		
6.74	1181.59	0.12	1201.68	0.09	1234.20	0.28		
7.05	1182.64	0.12	1203.41	0.10	1236.03	0.28		
7.33	1183.43	0.10	1204.65	0.09	1237.22	0.17		
7.53	1183.89	0.15	1205.74	0.09	1238.18	0.29		
7.87	1184.75	0.09	1207.33	0.11	1240.47	0.18		
8.29	1185.17	0.21	1209.62	0.29	1244.61	0.25		
8.49	1185.57	0.32			1246.21	0.13		
8.06	1183.86	0.40	1208.35	0.72	1244.98	0.11		

	c1-decompression series							
p	v107	SE	v113	SE	v192*	SE	v187	SE
7.98	105.76	0.59			192.60	0.07		
7.75					192.43	0.04		
7.56					192.03	0.03		
7.28					191.42	0.03		
7.05					190.94	0.04		
6.8					190.44	0.03		
6.55					189.86	0.11		
6.21					189.24	0.18		
6.04					188.81	0.11		
5.78					188.38	0.19		
5.48					187.76	0.09		
5.29					187.48	0.11		
4.98					186.82	0.15		
4.7					186.40	0.20		
3.78					185.58	0.10		
4.39	108.86	0.53	145.02	0.21	184.84	0.15	203.61	0.36
3.53	109.14	0.23	143.36	0.10	184.28	0.07	202.68	0.16
3.25	108.50	0.14	140.48	0.06	183.65	0.07	201.03	0.10
2.34	108.03	0.04	133.23	0.03	180.14	0.15	197.38	0.03
1.98	107.74	0.04	129.41	0.03	177.48	0.17	195.50	0.03
1.48	107.51	0.04	126.67	0.02	175.02	0.62	194.26	0.03
1.15	106.77	0.07	124.37	0.03	173.33	0.56	193.13	0.04

	c1-decompression series							
p	v231*	SE	v288*	SE	v392*	SE	v457*	SE
7.98	231.89	0.01	288.56	0.20	392.74	0.64	457.58	0.16
7.75	231.58	0.01	287.58	0.10	392.02	0.40	457.63	0.08
7.56	231.02	0.01	286.74	0.08	390.62	0.29	457.60	0.05
7.28	230.29	0.01	285.37	0.07	389.68	0.25	457.26	0.05
7.05	229.69	0.01	284.40	0.10	389.02	0.32	456.94	0.07
6.8	228.98	0.01	282.98	0.09	387.76	0.28	456.77	0.05
6.55	228.20	0.03	281.67	0.30	385.89	1.01	456.31	0.17
6.21	227.34	0.05	280.19	0.44	385.27	1.45	456.06	0.22
6.04	226.78	0.03	279.39	0.28	383.88	0.89	455.72	0.15
5.78	226.15	0.05	278.35	0.51	383.14	1.42	455.44	0.23
5.48	225.27	0.02	276.80	0.23	381.70	0.74	455.21	0.11
5.29	224.78	0.02	276.00	0.25	380.53	0.82	454.93	0.11
4.98	223.83	0.04	274.80	0.42	379.09	1.18	454.57	0.20
4.7	223.19	0.04	273.85	0.55	378.71	1.47	454.26	0.25
3.78	221.89	0.02	271.94	0.30	376.36	0.73	453.75	0.16
4.39	220.28	0.04	269.98	0.53	373.25	1.40	454.45	0.22
3.53	219.57	0.02	269.24	0.27	372.35	0.62	454.45	0.11
3.25	218.76	0.03	269.13	0.37	369.61	0.80	452.07	0.17
							461.23	0.23
2.34	217.93	0.33	277.68	0.43			460.24	0.04
1.98	217.08	0.27	277.46	0.38			459.97	0.04
1.48	217.72	0.35	276.00	0.41			460.12	0.06
1.15	214.52	0.43	274.89	0.54			460.08	0.06

	c1-decompression series							
p	v499*	SE	v498	SE	v604*	SE	v618*	SE
7.98	499.45	0.13			604.79	0.08	618.16	0.03
7.75	499.18	0.07			604.64	0.05	618.10	0.01
7.56	498.87	0.05			604.31	0.05	617.88	0.01
7.28	498.43	0.04			603.92	0.05	617.56	0.01
7.05	497.89	0.06			603.54	0.05	617.24	0.01
6.8	497.39	0.05			603.06	0.05	616.76	0.01
6.55	497.07	0.16			602.71	0.16	616.49	0.03
6.21	496.53	0.23			602.19	0.33	616.00	0.05
6.04	496.18	0.14			601.97	0.16	615.77	0.03
5.78	495.79	0.25			601.68	0.27	615.45	0.05
5.48	495.45	0.11			601.24	0.15	615.04	0.02
5.29	495.19	0.12			600.93	0.13	614.79	0.03
4.98	494.88	0.21			600.58	0.26	614.40	0.04
4.7	494.42	0.25			600.19	0.26	614.09	0.06
3.78	493.92	0.17			599.61	0.10	613.49	0.03
4.39	493.53	0.20	515.92	0.60				
3.53	493.29	0.10	514.90	0.26	598.48	0.13	612.76	0.05
					588.86	0.38	612.47	0.02
3.25	492.94	0.10	513.41	0.16				
2.34	491.44	0.22	508.73	0.06	589.91	0.16	611.68	0.03
					583.75	0.13	606.39	0.01
1.98	489.81	0.38	506.43	0.07	583.59	0.16	605.86	0.01
1.48			504.51	0.05	581.78	0.08	605.69	0.02
1.15			503.05	0.06	587.71	0.24	605.50	0.02
					581.00	0.09		

	c1-decompression series							
p	v706*	SE	v931	SE	v1052*	SE	v1056	SE
7.98	706.36	0.24			1052.08	0.01	1084.42	0.15
7.75	706.02	0.13			1051.27	0.00	1085.93	0.29
7.56	705.54	0.08			1050.68	0.00		
7.28	704.84	0.08			1049.54	0.00	1085.79	0.31
7.05	704.37	0.11			1048.57	0.00		
6.8	703.69	0.09			1047.54	0.00		
6.55	703.19	0.30			1046.22	0.01		
6.21	702.57	0.50			1044.98	0.02		
6.04	702.17	0.30			1044.28	0.01		
5.78	701.64	0.53			1043.33	0.02		
5.48	701.02	0.24			1042.20	0.01		
5.29	700.96	0.26			1041.50	0.01		
4.98	700.07	0.43			1040.60	0.01		
4.7	699.66	0.56			1039.69	0.01	1071.50	0.05
3.78	698.65	0.29			1037.88	0.01	1070.78	0.02
4.39	697.55	0.47	949.28	0.69	1036.37	0.01	1069.51	0.02
3.53	697.06	0.23	948.81	0.29	1035.71	0.01	1065.80	0.01
3.25	696.20	0.26	947.10	0.13	1034.41	0.01	1063.96	0.01
2.34			942.73	0.04	1031.55	0.05	1062.83	0.01
1.98			940.39	0.05	1029.74	0.08	1061.84	0.01
1.48			938.97	0.14				
1.15			937.47	0.11				

	c1-decompression series							
p	v1113*	SE	v1151	SE	v1157	SE	v1175	SE
7.98	1113.58	0.04						
7.75	1113.29	0.02						
7.56	1113.16	0.02						
7.28	1112.93	0.03						
7.05	1112.52	0.02						
6.8	1112.48	0.03						
6.55	1111.77	0.06						
6.21	1111.57	0.13						
6.04	1111.46	0.06						
5.78	1111.16	0.12						
5.48	1110.78	0.05						
5.29	1110.61	0.05						
4.98	1110.39	0.08						
4.7	1110.20	0.08						
3.78	1109.51	0.03						
4.39	1108.71	0.07	1155.07	0.40	1172.47	0.60	1188.03	0.72
3.53	1108.41	0.03	1154.99	0.18	1171.85	0.22	1186.75	0.31
3.25	1107.81	0.03	1154.17	0.13	1170.87	0.14	1184.79	0.16
2.34	1105.87	0.16	1152.96	0.07	1177.96	0.05		
1.98			1152.29	0.07	1175.22	0.05		
1.48			1151.99	0.06	1173.46	0.06		
1.15			1151.45	0.06	1171.86	0.07		

	c1-decompression series							
p	v1196	SE	v1244*	SE				
7.98			1244.74	0.09				
7.75			1244.09	0.05				
7.56			1243.61	0.03				
7.28			1242.72	0.03				
7.05			1242.05	0.04				
6.8			1241.12	0.03				
6.55			1240.49	0.09				
6.21			1239.56	0.16				
6.04			1239.18	0.09				
5.78			1238.47	0.16				
5.48			1237.60	0.07				
5.29			1237.16	0.07				
4.98			1236.45	0.11				
4.7			1235.80	0.15				
3.78			1234.59	0.06				
4.39			1232.94	0.10				
3.53			1232.32	0.05				
3.25	1218.41	0.15	1231.64	0.07				
2.34	1212.14	0.05						
1.98	1209.12	0.06						
1.48	1207.22	0.20						
1.15	1205.48	0.14						

Zusammenfassung

Kupfersulfat-Anhydrat, $CuSO_4$, Einkristalle wurden mit Hilfe von Diamantstempelzellen in Hochdruckexperimenten analysiert. Drücke bis zu ungefähr 8,5 GPa wurden während der Durchführung von Raman Spektrometrie und Röntgendiffraktometrie erreicht. Während Röntgendiffraktometrie keine Phasentransformation zweifelsfrei bestätigen konnte, zeigt Raman Spektrometrie Anzeichen für eine erste Phasentransformation bei ungefähr 1,5 GPa, welche eine Symmetriereduktion von Pnma nach $P2_1/c$ mit sich bringt. Zusätzlich konnte eine zweite Phasentransformation erster Ordnung zwischen 7 GPa und 8,5 GPa während der Kompression und zwischen 4,39 GPa und 1,98 GPa während der Dekompression festgestellt werden. Diese zeigt typische Merkmale einer Phasentransformation erster Ordnung mit einer deutlichen Hysterese und dem kritische Transformationsdruck P_c, welcher für jede Probe an einem anderen P auftritt. Eine Koexistenz von durchsetzten Nieder- und Hochdruck-Domänen ähnlich wie das Auftreten von Zwillingsdomänen und polysynthetische Verzwillingung kann angenommen werden. Diese zweite Phasentransformation kommt mit einer Symmetriereduktion von $P2_1/c$ to $P\bar{1}$.